Contribution of a deformable striking-ship structure to the structural crashworthiness of ship-ship collisions

Yeong Gook Ko[a], Sang Jin Kim[b], Jeom Kee Paik[a,b,c,*]

[a] Department of Naval Architecture and Ocean Engineering, Pusan National University, Busan 46241, Republic of Korea

[b] The Korea Ship and Offshore Research Institute (The Lloyd's Register Foundation Research Centre of Excellence), Pusan National University, Busan 46241, Republic of Korea

[c] Department of Mechanical Engineering, University College London, London, WC1E 7JE, UK

* Corresponding author. Tel.: +82-051-510-2429; fax: +82-051-518-7687.

E-mail address: jeompaik@pusan.ac.kr

Abstract

Ship-ship collision frequently occurs in shipping industry. The risks of economic losses and marine pollution have been increased by to ship-ship collisions especially involved with large oil tankers or liquefied natural gas (LNG)-fueled ships. Various type of methods are available for the purpose of safety studies in association with structural crashworthiness involving crushing and fracture in ship-ship collisions. In the perspectives of multi-physics and multi-criteria involved, however, the nonlinear finite element method is

1

certainly one of the most powerful techniques to model the problems. In a ship-ship collision accident where the bow of a striking ship is collided with the side of struck ship, the kinetic energy must be absorbed by both striking and struck ship structures in terms of collision damages and corresponding strain energies. As the bow structure of the striking ship is usually much stiffer than the side structure of the struck ship. It does not allow for deformation and damage. Therefore, no contribution of energy absorption is made by the striking structure. As the energy absorption characteristics of the striking ship depends on the structural arrangement of bulbous bow and flare, however, the contribution of striking ship cannot be entirely neglected. The aims of the present study are to examine the effects of a deformable striking ship structure on the structural crashworthiness of ship-ship collisions using LS-DYNA nonlinear finite element method computations. As an illustrative example in the paper, the struck ship is a VLCC class double hull oil tanker, while the struck ships are two types: a VLCC class tanker and a SUEZMAX class tanker. The relationships between collision forces versus penetration together with their energy absorption capabilities are characterized in association with the contributions of the striking ship bow where the deformable striking ship structures are compared with the rigid striking ship structures. Developed Findings and insights from the present study are summarized.

Introduction

Accidental limit states (ALS) potentially brings about a catastrophe of serious loss of life, and property or environmental damage. The aim of ALS design is to ensure that

the structure is able to withstand specified accidental events such as collision, grounding, fire and explosion and to enable evacuation of personnel from the structure for a sufficient period under specific environmental conditions after accidents occur (Paik and Thayamballi 2003, 2007).

Limit state design and safety assessment relevant to collisions and grounding are generally based on the energy absorption capability of the structure until accidental limit state is reached. As the energy absorption capability can be calculated by integration of the area below the reaction force versus penetration curve of the structure, the improving structural crashworthiness of the ships must be fulfilled to obtain those curves in the accidental event.

As the amount of energy dissipation at the fore part of the striking ship is relatively lower than at the side part of the struck ship, conservative evaluations are relevant especially for safety designs in general, most ship collision simulations have been undertaken in the past where striking ships were modelled as a rigid body (Ammerman and Daidola 1996, Wisniewski and Kolakowski 2002, Haris and Amdahl 2011, Montewka et al. 2012, Sun et al. 2015, Zhang et al. 2016). On the other hand, some other studies have of course been conducted with the striking ships that were modelled as a deformable body (Hogström and Ringsberg 2012, Haris and Amdahl 2013, Storheim and Amdahl 2015), however it is observed that more efforts are recommended to examine the contribution of a realistic striking ships to the structural crashworthiness of ship-ship collisions.

The aim of this study is to investigate the effects of a deformable striking-ship structure on the structural crashworthiness in ship-ship collisions. The characteristics of the energy absorption capabilities of ship structures in collision or grounding were studied in the literature by many investigators using the non-linear finite element method (Amdahl 1983, Simonsen 1997, Zhang 1999, Tornqvist 2003, Urban 2003, Alsos 2008, Hong 2009, Ehlers et al. 2010, 2016, Storheim and Amdahl 2015). This study also uses the non-linear finite element method with the LS-DYNA code (Hallquist 2010).

Collision Scenarios

Among various type of ships, the oil tanker which can bring about a significant amount of pollution has been utilized as a target structure in the simulations and a host of researchers have fulfilled studies with oil tankers to reduce loss of financial properties and to prevent loss of lives and environmental damages (Zheng et al. 2007, Tavakoli et al. 2010, Kim et al. 2015, Faisal et al. 2016, Parunov et al. 2016, Youssef et al. 2014, 2017).

In the present study, it is considered that the side structure of a VLCC class double-hull oil tanker is collided with the bow structure of either a VLCC class double-hull oil tanker or a SUEZMAX class double-hull oil tanker. Tables 1 and 2 indicate the principal dimensions of the both ships. Figure 1 shows the finite element models.
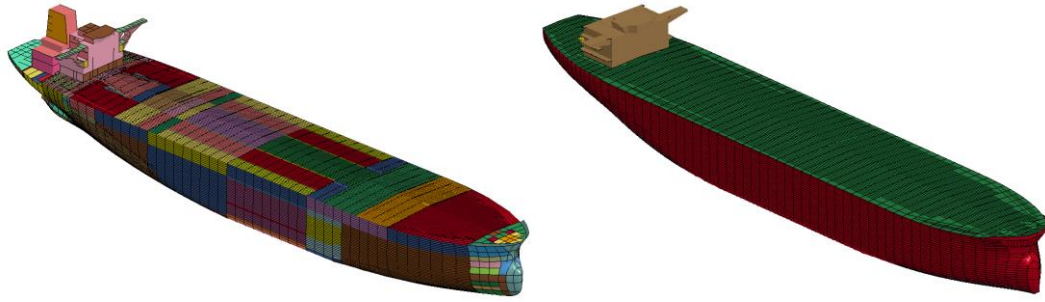
4

Figure 1. The VLCC class (left) and SUEZMAX class (right) double-hull oil tankers.

Table 1. Principal dimensions of the VLCC class double-hull hull oil tanker.

Parameter	Dimension
Overall length (m)	318.2
Moulded breadth (m)	60
Moulded depth (m)	30
Moulded draught (m)	21.6
Dead weight (ton)	300,000
Transverse frame spacing (m)	5.69

Table 2. Principal dimensions of the SUEZMAX class double-hull oil tanker.

Parameter	Dimension
Overall length (m)	272.0
Moulded breadth (m)	48.0
Moulded depth (m)	23.7
Moulded draught (m)	16.0
Dead weight (ton)	157,500
Transverse frame spacing (m)	4.8

For the present study, the colliding angle between the striking and struck ships as denoted in Figure 2 is varied at θ = 45, 90 and 135 degrees. The speed of the striking ships is varied at V_2 = 0.5, 3, 6 and 10 knots, while the struck ship is standstill at V_1 = 0 knot. The location of collision is around midship (No. 3 cargo hold) of the struck ship. Also, it is assumed that both striking and struck ships at the time of collision are in the laden (fully loaded) condition. Table 3 indicates a summary for a total of 48 cases studied with varying the collision conditions considered in the present study.
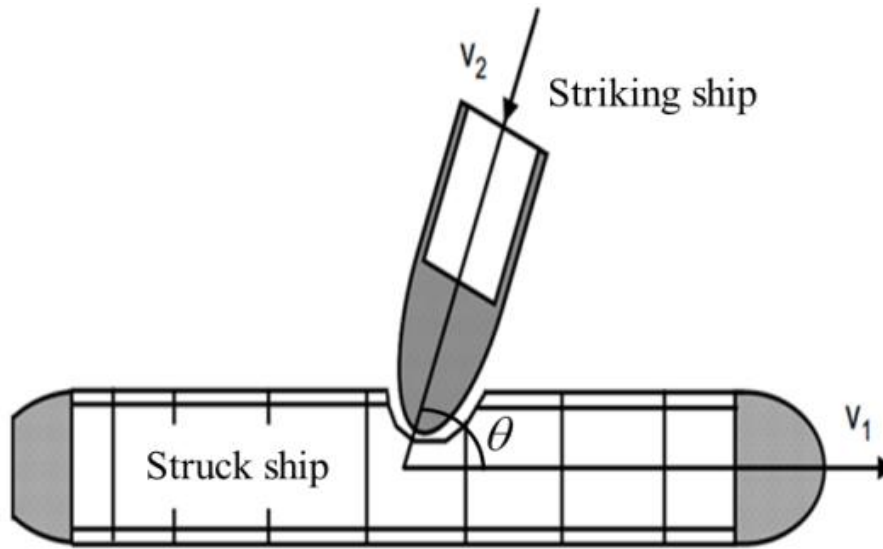
Figure 2. Definition of the collision angle between the striking and struck ships.

Table 3. Case study identification numbers with varying the collision conditions.

Case No.	Striking ship	Rigid or deformable	Collision angle θ (deg.)	Collision speed V_2 (knot)
1~12	VLCC	Rigid	90, 45, 135	0.5, 3, 6, 10
13~24	VLCC	Deformable	90, 45, 135	0.5, 3, 6, 10
25~36	SUEZMAX	Rigid	90, 45, 135	0.5, 3, 6, 10
37~48	SUEZMAX	Deformable	90, 45, 135	0.5, 3, 6, 10

Nonlinear Finite Element Method Modelling

3.1 Material Property Modelling

The striking and struck ship structures are made of both mild and high tensile steels.

The mechanical properties of mild and high tensile steels (AH32 and AH36) are

indicated in Table 4. In the present LS-DYNA simulations, the elastic-perfectly

plastic material model is applied without considering the strain-hardening effect. The

material option of "Mat.024-Elastic/Plastic Isotropic with piecewise linear

plasticity" is adopted to consider the dynamic effects such as strain-rate sensitivity in

yield strength and fracture strain (ISSC 2003, 2012, Sajdak and Brown 2004, Paik 2007a, 2007b, Yamada and Endo 2008).

Table 4. Material properties of the striking and struck ship structures.

Material property		Mild steel	High-tensile steel	
			AH32	AH36
Density, ρ (ton/m^3)		7.85	7.85	7.85
Young's modulus, E (MPa)		205,800	205,800	205,800
Poisson's ratio		0.3	0.3	0.3
Yield stress, σ_Y (MPa)		235	315	355
Cowper-Symonds coefficient	C	40.4	3200	3200
	q	5	5	5

3.2 Finite Element Size

As the structural crashworthiness in ship-ship collisions involves crushing and fracture, it is important to assign relevant mesh sizes in the finite element method modelling. In the present study, only plate-shell elements with an aspect ratio of almost unity were used but without beam elements. For the structural areas that are less affected by the collision, coarse meshes were used. The plating was modelled with an element size of 1 m. The stiffener webs were modelled by one element while stiffener flanges were modelled by one element for an angle type and two elements for a T-type girder.

On the other hand, the collided areas were modelled by fine meshes. Paik and Thayamballi (2003, 2007) and Paik (2007a, 2007b) suggested techniques to define relevant size of finite elements to compute the structural crashworthiness of thin-walled structures when a rectangular type of plate-shell elements is utilized. The element size can then be determined from Equation (1) to represent the crushing

behavior of thin walls as illustrated in Figure 3.

$$s \leq \frac{H}{8} = 0.1228b^{2/3}t^{1/3} \tag{1}$$

where s is the element size, H is the half-fold length which may be taken as

$H = 0.983b^{2/3}t^{1/3}$ (Wierzbiki and Abramowicz 1983), b is the plate breadth between

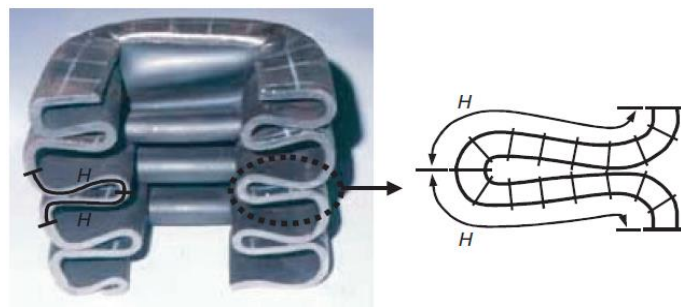support members (e.g., stiffeners, frames, stringers), and t is the plate thickness.

Figure 3. Definition of the half-fold-length of a thin-walled structure crushed under predominantly axial compression and cut at its midsection (Paik and Thayamballi 2007).

In the present study, the above-mentioned Paik-Thayamballi method yields an element size of between 104 - 244 mm, depending on the breadth and thickness of plate at different areas for the element size as indicated in Table 5. To reconfirm this value, a convergence study was performed by varying the element size. Figure 4 shows the results of the convergence study in terms of penetration and absorbed energy of the struck ship structures. The collision between a striking VLCC tanker and a struck VLCC tanker was considered with a collision angle of 90 deg. at a collision speed of 2 knots. The collision also between a striking SUEZMAX tanker

and a struck VLCC tanker was also analysed for the convergence study. As a result, it

was realized that the trend is quite similar. It is concluded from the convergence

studies that the prediction of the mesh size by the Paik-Thayamballi method is good

enough and the element size was finally taken as 200 mm in the present study.
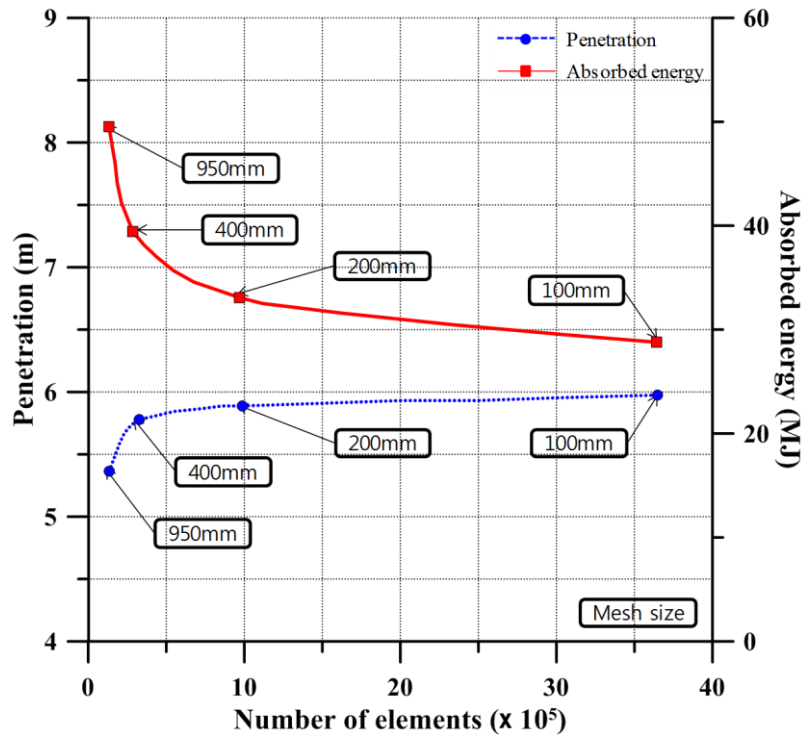
Figure 4. The convergence study to determine the element size

Table 5. Applied element sizes.

Area	Breadth of plate b (mm)	Plate thickness t (mm)	A half-fold length H (mm)	Element size s (mm)
Frame space	5690	18.5	828.61	103.68
Deck height	6600	24	997.67	124.84
Hull depth (except double bottom)	20608	18.5	1954.2	244.52

3.3 Dynamic Yield Strength

The dynamic yield strength of material is determined from the Cowper-Symonds

equation (2).

$$\sigma_{Yd} = \left[1 + \left(\frac{\dot{\varepsilon}}{C}\right)^{1/q}\right]\sigma_Y \tag{2}$$

where σ_Y and σ_{Yd} are the static and dynamic yield stresses, respectively, $\dot{\varepsilon}$ is the strain rate, and C and q are the Cowper-Symonds coefficients. The coefficients in Equation (2) are taken as indicated in Table 4, where it is noted that they differ for mild and high tensile steels (Paik 2007a, 2007b).

3.4 Dynamic Fracture Strain

In the present study, the dynamic fracture strain of material used is determined from the method developed by the authors (Ko et al. 2017). Figure 5 describes the method to determine the dynamic fracture strain ε_{fd} where the static fracture strain ε_{fc} is determined as a function of the static fracture strain ε_f of material determined from the tensile coupon test. The dynamic fracture strain to be used for nonlinear finite element method computations is then determined as an inverse of the Cowper-Symonds equation as indicated in Equation (3) (Paik and Thayamballi 2003, Paik 2007a, 2007b).

$$\varepsilon_{fd} = \left[1 + \left(\frac{\dot{\varepsilon}}{C}\right)^{1/q}\right]^{-1}\varepsilon_{fc} \tag{3}$$

where ε_{fc} and ε_{fd} are the static and dynamic fracture strains to be used for nonlinear finite element method computations, respectively, $\dot{\varepsilon}$ is the strain rate, and C and q are the Cowper-Symonds coefficients which are taken as indicated in Table 4.
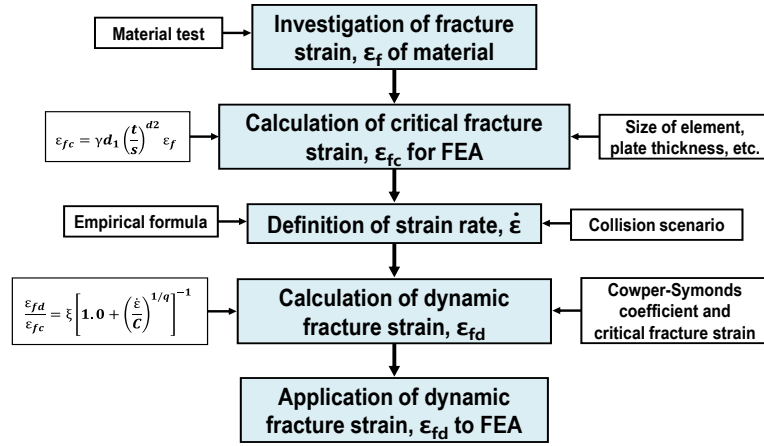
Figure 5. Procedure to determine the dynamic fracture strain to be used for nonlinear finite element method computations (Ko et al. 2017).

Using Equation (3), Ko et al. (2017) suggested to determine the strain rate $\dot{\varepsilon}$ as a function of the collision speed as follows:

$$\dot{\varepsilon} = 1.528V_2 - 0.686 \tag{4}$$

where V_2 is the collision speed in knot of the striking ship.

In the present study, 0.43 and 0.32 of static fracture strain obtained from experiments are used. Table 6 indicates a summary of dynamic fracture strains determined from the above-mentioned method. The plate thickness also affects the fracture strains, therefore, the dynamic fracture strains must differ for different plates with different thicknesses. However, it is interesting to note that the dynamic fracture strain is close to 0.1 which is well adopted in the industry practice, but it is seen that the method of Ko et al. (2017) gives a reasonable guidance to determine the dynamic fracture strains in general scenarios.

Table 6. The dynamic fracture strains used for the nonlinear finite element method computations.

Collision speed V_2 (knot)	Strain rate $\dot{\varepsilon}$ (1/sec)	Steel grade	Static fracture strain ε_f	Critical fracture strain ε_{fc}	Dynamic fracture strain ε_{fd}	Dynamic yield stress σ_{Yd}
0.5	0.079	Mild steel	0.43	0.129	0.100	302.416
		High tensile steel	0.32	0.096	0.086	352.692
3	3.901	Mild steel	0.43	0.129	0.079	382.240
		High tensile steel	0.32	0.096	0.076	397.322
6	8.488	Mild steel	0.43	0.129	0.074	407.010
		High tensile steel	0.32	0.096	0.074	411.170
10	14.604	Mild steel	0.43	0.129	0.071	426.728
		High tensile steel	0.32	0.096	0.072	422.195

3.5 Contact Problem Modelling

Thin-walled structural components contact each other during crushing. Therefore, the structural crashworthiness analysis needs to model contact problems properly. Typically, two types of contact are considered, general contact and self-contact. The former is affected by surfaces between different structural components, while the latter can arise from structural components themselves due to folding or crushing. It is obvious that the effect of overlapping of contacted surfaces can be of significance. In the present study, the contacts between the striking and struck vessels are applied as in LS-DYNA "Automatic Surface to Surface" for general contact and "Automatic Single Surface" for self-contact. The effects of self-contact phenomenon are often omitted for saving computational times in simulations. In the present LS-DYNA computations, however, both general contact and self-contact are taken into account.

3.6 Friction Effect Modelling

During collision, the effect of friction can not be neglected if there is a relative

velocity between the striking and struck bodies. The influence of friction may be of significance for a collision where the contact occurs at the side of the struck ship like a racking type (Paik and Thayamaballi 2007). In the present study, however, a friction constant of 0.3 is assumed for all collision scenarios. This is a simple assumption. However, it should be noted that the characteristics of friction may change even in the same collision scenario as the penetration proceeds. In this regard, further studies are recommended.

3.7 Surrounding Water Effect Modelling

the vessels are moving on the ocean at the time of collision accidents, and thus striking and struck vessels are not fixed in any direction where they naturally move even after collisions. For this reason, the external ship dynamics should be considered, and it is defined with respect to hydrodynamics and the ship motions. The ship hydrodynamics denote the surrounding water effect in terms of added masses, and the ship motions are calculated by carrying rigid-body motion analysis out. In addition, the effect of sea water (e.g., added mass) against vessel's motions cannot be neglected as a part of kinetic energy is consumed for the movement of the ships involved.

For the present nonlinear finite element method computations, free body boundary condition is applied by using LS-DYNA/MCOL program which can simulate a ship motion taking into account the effect of the added mass during collision (Kuroiwa et al. 1995, Kuroiwa 1996, Kitamura 2000, Ferry et al. 2002, Le Source et al. 2003). In

this modelling, the effect of surrounding water is taken into account in terms of

hydrodynamic forces associated with the deceleration of the ships where a virtual

mass of the striking and struck ships in surge, sway and yaw motions is added to the

actual ship mass. The motions of pitch, roll and heave may be neglected because of

relatively lower effects to the computation results than the surge, sway, and yaw

directions.

Upon using the LS-DYNA/MCOL solver for ship-ship collisions, the resultant forces

and moments imposed on the struck ship structure are calculated at each time step

during the simulation, and by using these values the new position of the struck ship is

then updated without additional boundary conditions as shown in Figure 6. In the

present computations, $c_{11} = 0.05$, $c_{22} = 0.85$, and $c_{33} = 0.21$ in Equation (5) are

taken for the movements of the struck ship at each direction (Pedersen and Zhang

1998).

$$a_{11} = c_{11}m_2, \quad a_{22} = c_{22}m_2, \quad a_{33} = c_{33}I_2 \tag{5}$$

where a_{11}, a_{22} and a_{33} are the added masses in the direction of surge, sway and

yaw motions, respectively, c_{11}, c_{22} and c_{33} are the coefficients of added masses

for each motion, m_2 is the mass of struck vessel, and I_2 is the mass moment of

inertia of struck vessel.
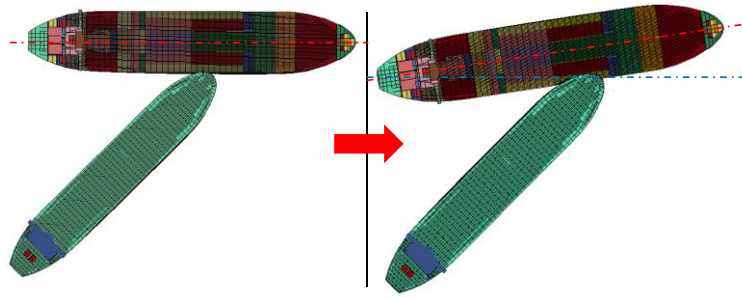
Figure 6. Motion of struck ship before (left) and after (right) collision in LS-DYNA/MCOL simulations.

Results and Discussions

In the present study, LS-DYNA computations have been performed for total 48 cases addressed in Table 3. Various results are obtained including deformations, stresses, and resultant forces of both striking and struck ship structures. The relationships between resultant forces versus time, and between penetration versus time are firstly identified from the numerical computations. Using these relations, resultant forces versus penetration curves are then obtained, where resultants forces and penetration are taken at the identical time each other. The relationships between absorbed energy versus penetration can then be obtained by integrating the areas below the corresponding curves.

Maximum penetration is one of primary concerns as the bow structure of striking ship penetrates the side structure of struck ship. In the present study, a reference penetration was measured for the maximum sideways penetration of struck ship's cargo hold number 3 or for the maximum deformation of striking ship's bulbous bow tip along the ship's longitudinal direction. According to Paik and Pedersen (1995),

resultant forces on the struck and striking vessels should be on equilibrium. Hence, the amount of damage is to be calculated in facet of the penetration for colliding and collided structures as well as absorbed energy as a result of collision accident can be calculated by integral of resultant force. For this reason, table 7 indicates a summary of maximum penetration together with the corresponding maximum resultant forces and absorbed energy until all the kinetic energy is entirely consumed.

Table 7. Maximum structural consequence.

Case	Collision angle θ (deg.)	Collision speed V_2 (knot)	Max. penetration (m)	Max. absorbed energy (MJ)	Max. resultant force (MN)
1	90	0.5	0.192	2.596	8.288
2	90	3	3.735	61.009	30.694
3	90	6	8.710	220.528	36.389
4	90	10	20.920	484.870	45.280
5	45	0.5	0.081	0.309	3.739
6	45	3	1.232	19.907	23.068
7	45	6	2.763	102.343	40.857
8	45	10	3.660	322.774	61.007
9	135	0.5	0.062	0.266	3.698
10	135	3	1.464	18.741	21.626
11	135	6	2.368	167.532	39.441
12	135	10	17.190	644.734	56.082
13	90	0.5	0.182	2.406	8.068
14	90	3	3.005	32.859	25.464
15	90	6	4.760	131.688	47.039
16	90	10	7.100	342.360	61.860
17	45	0.5	0.101	0.239	1.759
18	45	3	0.142	8.247	29.728
19	45	6	0.513	44.183	47.207
20	45	10	1.690	117.224	61.207
21	135	0.5	0.092	0.236	1.688
22	135	3	0.084	9.991	22.696
23	135	6	0.318	44.402	45.831
24	135	10	2.320	170.164	57.152
25	90	0.5	0.132	2.016	9.478
26	90	3	3.455	50.609	30.014
27	90	6	8.150	174.988	33.879
28	90	10	21.780	412.030	35.080

29	45	0.5	0.001	0.009	0.879
30	45	3	0.442	9.747	15.198
31	45	6	0.973	82.043	26.467
32	45	10	3.780	291.144	45.857
33	135	0.5	0.002	-0.004	1.088
34	135	3	0.214	9.211	15.806
35	135	6	2.968	122.102	26.971
36	135	10	10.730	402.244	44.842
37	90	0.5	0.142	1.966	9.418
38	90	3	3.095	42.709	29.114
39	90	6	6.780	154.778	35.629
40	90	10	16.410	345.510	40.410
41	45	0.5	0.011	0.039	2.199
42	45	3	1.012	12.257	24.678
43	45	6	1.943	84.693	38.387
44	45	10	3.300	313.464	54.997
45	135	0.5	0.012	0.016	2.158
46	135	3	1.254	9.991	22.696
47	135	6	2.228	87.432	39.311
48	135	10	5.410	303.404	50.732

Figures 7 and 8 show deformed shapes of the VLCC tanker structures struck by the VLCC and the SUEZMAX tanker structures with a deformable and rigid bow, where collision angles are varied while the collision speed was fixed at 10 knots. The deformations of side structures were measured at around the tip of the striking bow. It is evident that the damage extent and the amount of side structures struck by a rigid striking bow are much larger than those struck by a deformable striking bow.
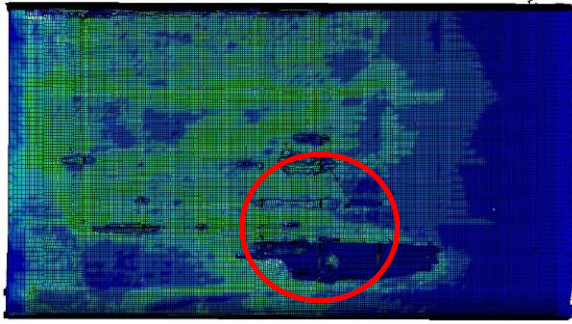
(a) Deformable bow at a collision angle of 45 deg.
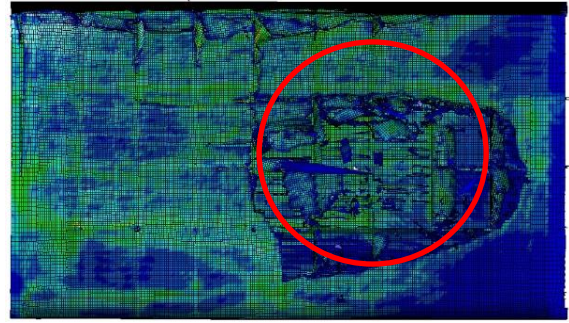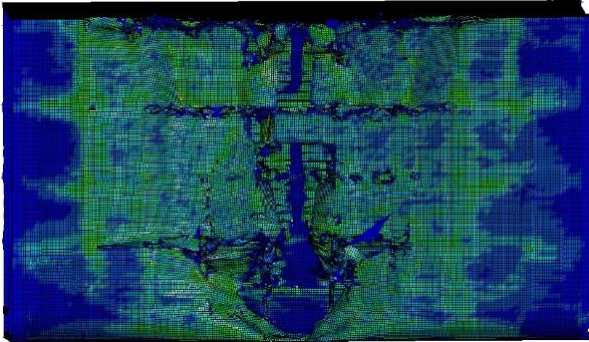
(b) Rigid bow at a collision angle of 45 deg.

(c) Deformable bow at a collision angle of 90 deg.
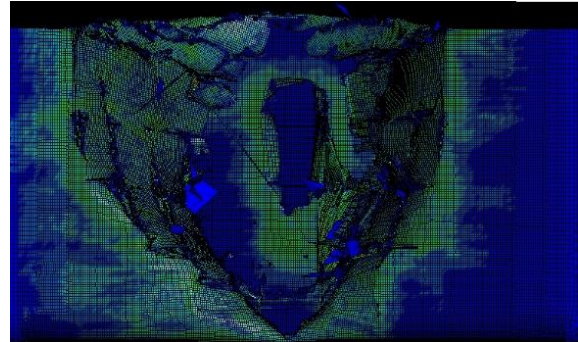
(d) Rigid bow at a collision angle of 90 deg.
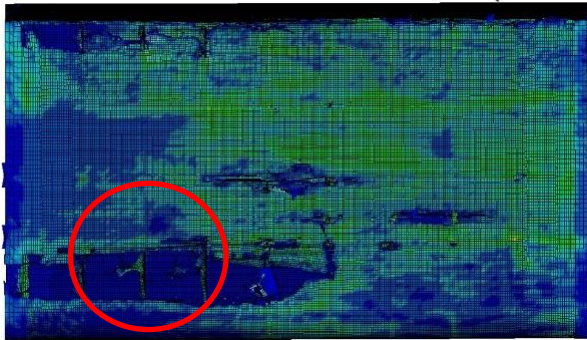
(e) Deformable bow at a collision angle of 135 deg.
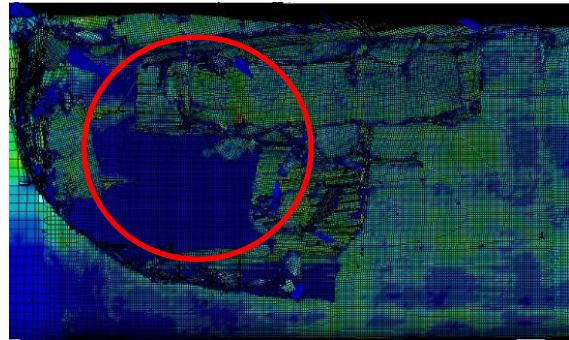
(f) Rigid bow at a collision angle of 135 deg.

Figure 7. Deformed shapes of struck VLCC tanker at around the tip of striking VLCC bow with a collision speed of 10 knots.
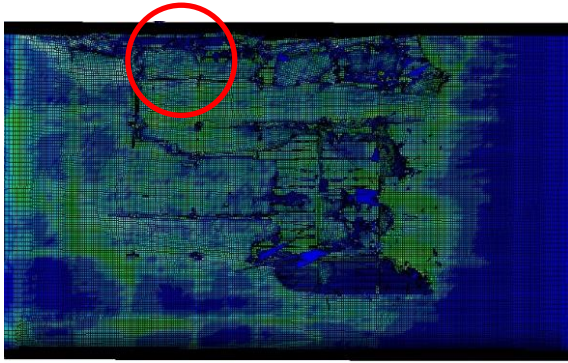
(a) Deformable bow at a collision angle of 45 deg.
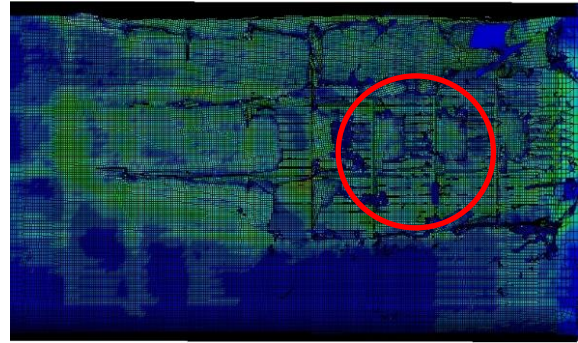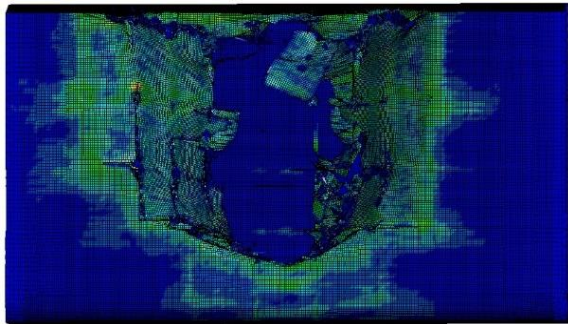
(b) Rigid bow at a collision angle of 45 deg.

(c) Deformable bow at a collision angle of 90 deg.
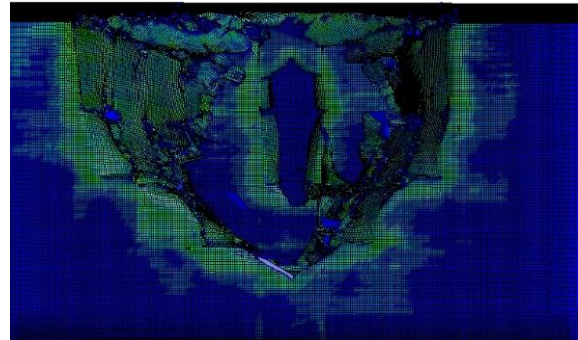
(d) Rigid bow at a collision angle of 90 deg.
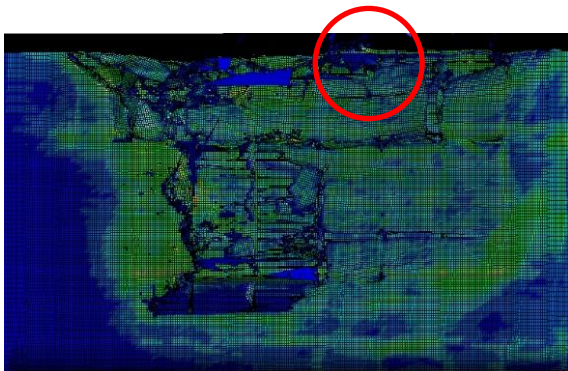
(e) Deformable bow at a collision angle of 135 deg.
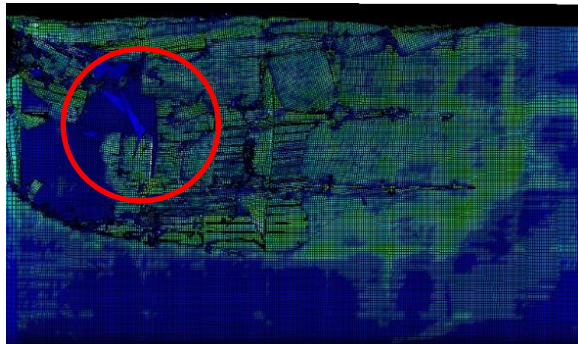
(f) Rigid bow at a collision angle of 135 deg.

Figure 8. Deformed shapes of struck VLCC tanker at around the tip of striking SUEXMAX bow with a collision speed of 10 knots.

Figures 9 and 10 show the relationships between resultant forces and absorbed energies versus penetration in conjunction with Figures 7 and 8. It is found that at a collision angle of 90 deg., the differences between the deformable and rigid bows are

relatively small in terms of the rupture or perforation of outer and inner shell plate

panels. This means that the industry practice in the treatment of striking ship bow as a

rigid body may still be useful as far as the rupture of outer and inner shell plate panels

are concerned. However, the differences between the deformable and rigid bows are

of significance in terms of the structural crashworthiness associated with the

maximum penetration and the total volume of damages which are related to the speed

and amount of oil spills. This is because the remaining kinetic energy after the rupture

of inner shell plate panels is further consumed by damaging not only the struck-ship

side structures but also the striking-ship bow structures. Considering that the

deformable bow model is more realistic and accurate, it is recommended that the rigid

striking bow model applied in the current industry practice should not be used.
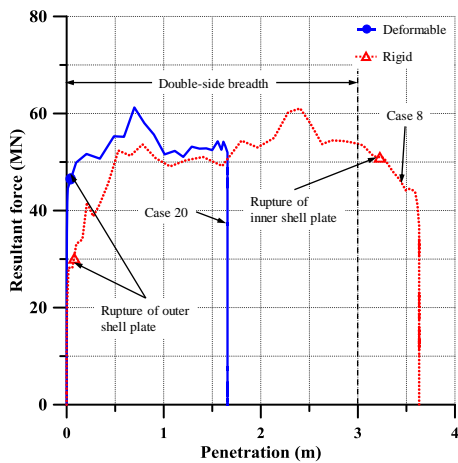
(a) Collision angle of 45 deg.   (b) Collision angle of 45 deg.
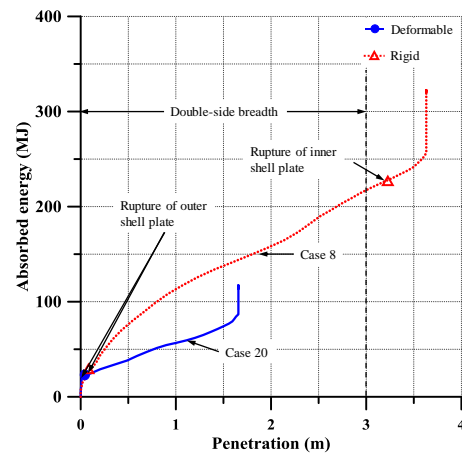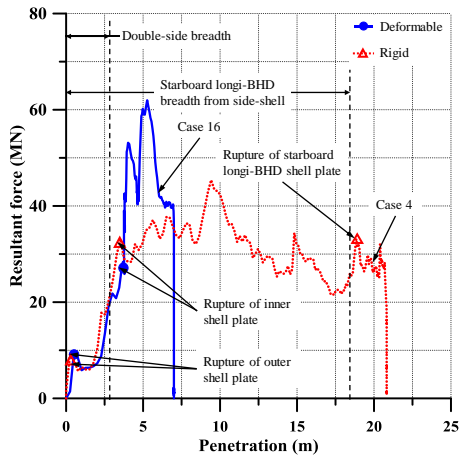
(c) Collision angle of 90 deg.
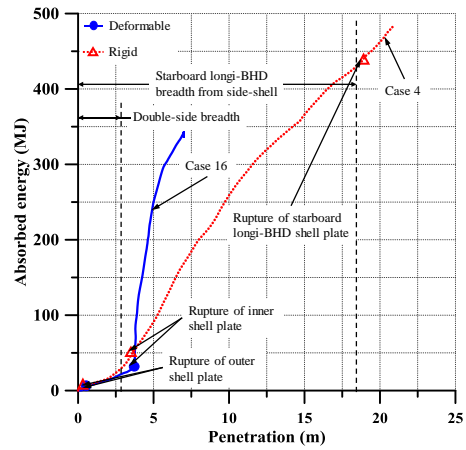
(d) Collision angle of 90 deg.
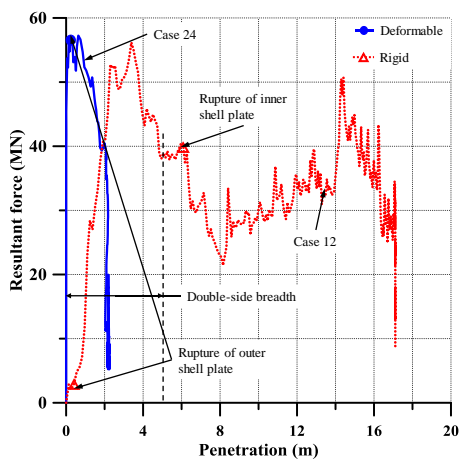
(e) Collision angle of 135 deg.
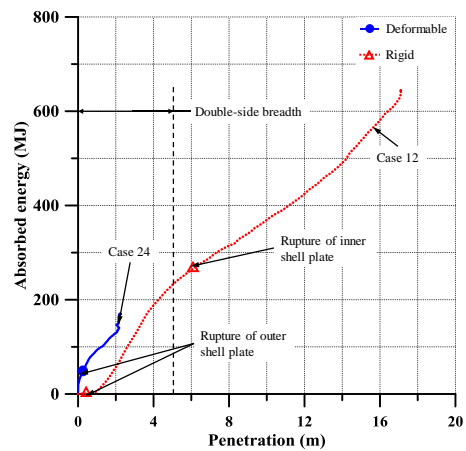
(f) Collision angle of 135 deg.

Figure 9. The relationships between resultant forces or absorbed energies versus penetration for the VLCC tanker struck by the VLCC tanker at a collision speed of 10 knots.

(a) Collision angle of 45 deg.

(b) Collision angle of 45 deg.

(c) Collision angle of 90 deg.

(d) Collision angle of 90 deg.

(e) Collision angle of 135 deg.

(f) Collision angle of 135 deg.
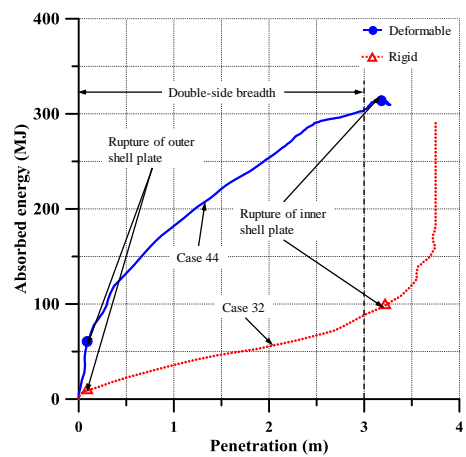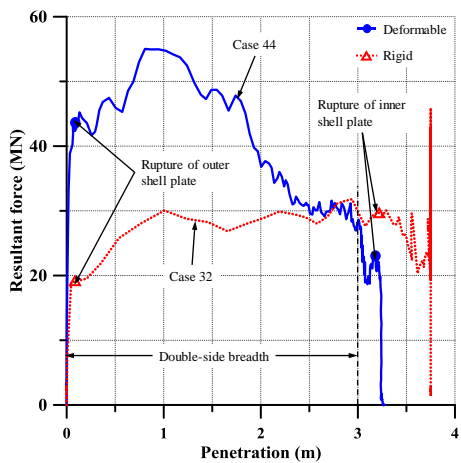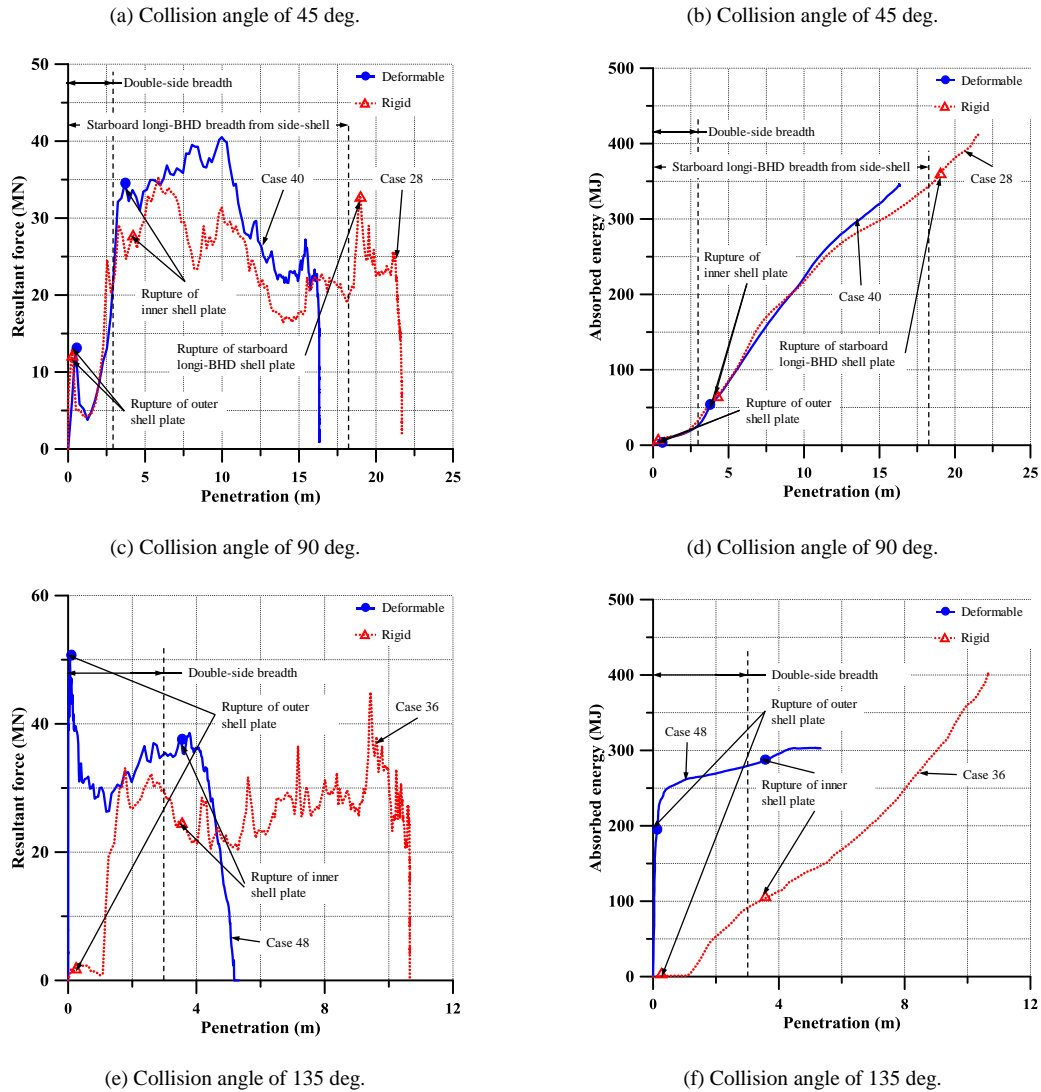
Figure 10. The relationships between resultant forces or absorbed energies versus penetration for the VLCC tanker struck by the SUEZMAX tanker at a collision speed of 10 knots.

The stiffness of bulbous bow is generally higher than the side structure of the struck vessel. Thus, the influence of a deformable bulbous bow should be considered (Ehlers and Tabri 2012). The behavior of penetration or resultant forces with time for the striking VLCC or SUEZMAX tanker at each collision angle were illustrated in Appendix A to compare the results between striking and struck vessels. Figure 11

shows some example of the behaviors of the deformable and rigid striking ship bow on the maximum penetration, maximum absorbed energy. As shown in Figure 11 (a). the rigid bow penetration lengths between SUEZMAX and VLCC are significantly different except the case at collision speed of 10 knots contrast to Figure 11 (c) which shows that those are nearly equal. That is because it stems from the shape of vessel fore part. Even though the fore part of the SUEZMAX is sharper than VLCC, the rigid bow penetration lengths appears almost the same at the collision angle of 90 degree because of the difference in initial kinetic energy, which is influenced by the displacement of the vessel. In addition, relatively low difference of the absorbed energy between collision angles of 45 and 90 degree also can be seen in Figure 11. It seems that the shape of vessel fore part can affect to the damage pattern and extent. The behaviors of the deformable and rigid striking ship bow on the maximum penetration, maximum absorbed energy and maximum resultant forces with varying angle or speed of collision are shown in Appendix B and C. It is found from these results that the effects of the deformable striking ship bow are of significance as the collision speed increases. Also, the maximum penetration occurs at the collision angle of 90 deg. It is again obvious from these computations that the deformable striking ship bow structures absorb some part of the initial kinetic energy of the collision as they penetrate into the struck ship structures in contrast to the industry practice applied with a rigid body.
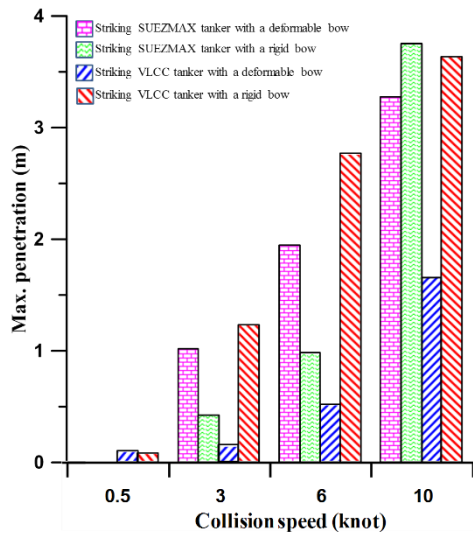
(a) 45 deg.
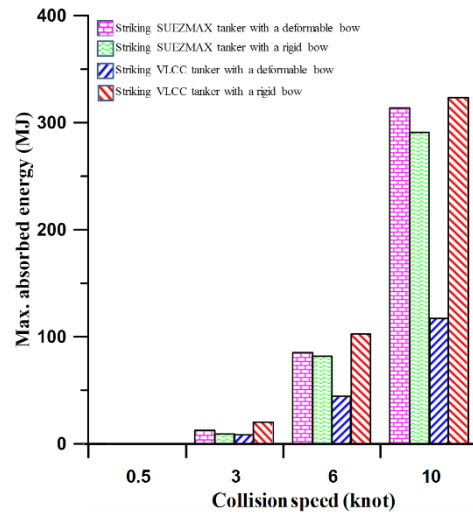
(b) 45 deg.
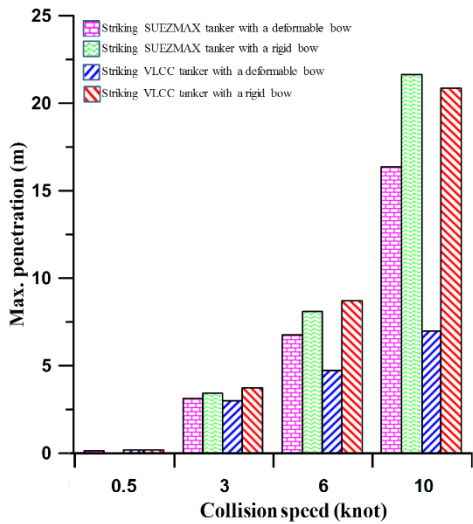
(c) 90 deg.
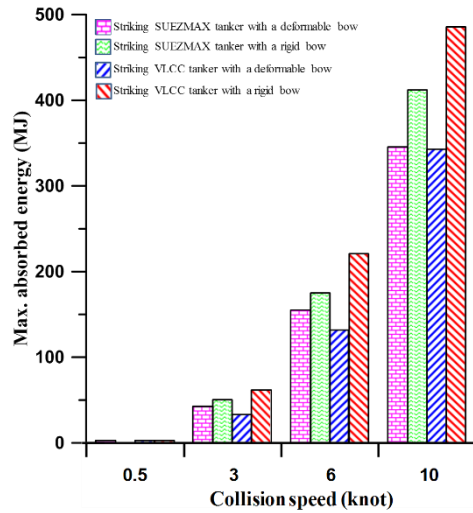
(d) 90 deg.

Figure 11. Some example of the behaviors of the deformable and rigid striking ship bow on the maximum penetration, maximum absorbed energy

Concluding Remarks

The aim of the present paper has been to examine the effects of a deformable striking ship bow in ship-ship collisions. An extensive study of nonlinear finite element method computations has been undertaken for given collision scenarios in association

with the structural crashworthiness. The angle of collision was varied at 45, 90, and 135 deg. The speed of collision was also varied at 0.5, 3, 6 and 10 knots. The collision location was fixed at the center of the number 3 cargo hold of the struck VLCC tanker. Also, both striking and struck ships were considered as a full load condition that can affect the collision location in elevation. A total of 48 scenarios were analyzed by the LS-DYNA nonlinear finite element method. In the industry practice, the striking ship bow is often modeled as a rigid body, but the present study modeled the striking ship bow as a deformable body with the realistic properties of geometry and materials. For a comparison purpose, the rigid body model of the striking ship bow was also considered. Based on the present study, important insights and conclusions can be drawn as follows:

(1) The rigid bow model of the striking ship results in a greater penetration than the deformable bow model of the striking ship as the striking ship bow structures absorb some part of the initial kinetic energy in the latter model.

(2) The penetration is the largest at the collision angle of 90 deg. as would be expected.

(3) The difference of the structural crashworthiness between the deformable and rigid bow models becomes larger as the collision speed increases.

(4) The shape of the striking ship bow affects the structural damage patterns and the resulting penetration. As the shape of the striking SUEZMAX tanker bow is sharper than that of the striking VLCC tanker bow, the maximum

penetration of the former is larger than the latter without regard to the fact that the initial kinetic energy of the VLCC tanker is greater than that of the SUEZMAX tanker. Because the displacement of the VLCC is larger than that of the SUEZMAX.

(5) At a collision angle of 90 deg., the difference between the deformable striking-ship bow model and the rigid striking-ship bow model is relatively small until the outer and inner shell plate panels rupture. However, the behavior with the deformable striking-ship bow model is totally different from that with the rigid striking-ship bow model after the rupture of the outer and inner shell plate panels or at other collision angles in terms of the maximum penetration and the total volume of structural damages which are related to the speed and amount of oil spills.

(6) In general, the effects of the deformable striking ship bow are significant in terms of penetration, absorbed energy amount and resultant forces. It should not be neglected in the analysis of structural crashworthiness in ship-ship collisions. Significance becomes greater as the collision speed becomes faster.

References

Alsos HS. 2008. Ship grounding: analysis of ductile fracture, bottom damage and hull girder response [PhD thesis]. Norwegian University of Science and Technology, Trondheim, Norway.

Amdahl J. 1983. Energy absorption in ship-platform impacts [PhD thesis]. Norwegian University of Science and Technology, Trondheim, Norway.

Ammerman DJ, Daidola JC. 1996. A comparison of methods for evaluating structure during ship collision. Sandia National Labs., Albuquerque, New Mexico, USA

ANSYS/LS-DYNA. User's manual for ANSYS/LS-DYNA. Version 14.5, ANSYS Inc., New York, USA.

Bin S, Hu Z, Wang G. 2015. An analytical method for predicting the ship side structure response in raked bow collisions. *Marine Structure*. 41: 288-311.

Buldgen L, Le Sourne H, Besnard N, Rigo P. 2012. Extension of the super-elements method to the analysis of oblique collision between two ships. *Marine Structure*. 29: 22-57.

Cowper GR, Symonds PS. 1957. Strain-hardening and strain-rate effects in the impact loading of cantilever beams. Technical Report No. 28, Division of Applied Mathematics, Brown University, Providence, USA.

Ehlers S, Guiard M, Kubiczek J, Hoderath A, Sander F, Sopper R, Charbonnier P, Marhem M, Darie I, von Selle H, Peschmann J, Bendfeldt P. 2016. Experimental and numerical analysis of a membrane cargo containment system for liquefied natural gas. *Ships and Offshore Structures*. 12(S1): S257-S267.

Ehlers S, Tabri K. 2012. A combined numerical and semi-analytical collision damage assessment procedure. *Marine Structures*. 28: 101-119.

Ehlers S, Tabri K, Romanoff J, Varsta P. 2010. Numerical and experimental investigation on the collision resistance of the X-core structure. *Ships and Offshore Structures.* 7(1): 21-29.

Faisal M, Noh SH, Kawsar MRU, Youssef SAM, Seo JK, Ha YC, Paik JK. 2016. Rapid hull collapse strength calculations of double hull oil tankers after collisions. *Ships and Offshore Structures.* 12(5): 624-639.

Ferry M, Le Sourne H, Besnier F. 2002. MCOL-Theoretical Manual. Technical Report No. 01-52, French Shipbuilding Research Institute, Nantes, France.

Hallquist JO. 2010. LS-DYNA 3D Theory manual. Livermore Software Technology Corporation, CA, USA.

Haris S, Amdahl J. 2011. An analytical model to assess a ship side during a collision. *Ships and Offshore Structures.* 7(4): 431-448.

Haris S, Amdahl J. 2013. Analysis of ship-ship collision damage accounting for bow and side deformation interaction. *Marine Structures*. 32: 18-48.

Hogstrom P, Ringsberg JW. An extensive study of a ship's survivability after collision – A parameter study of material characteristics, non-linear FEA and damage stability analyses. *Marine Structures*. 27: 1-28.

Hong L. 2008. Simplified analysis and design of ships subjected to collision and grounding. Norwegian University of Science and Technology, Trondheim, Norway.

Hong L. 2009. Simplified analysis and design of ships subjected to collision and grounding [PhD thesis]. Norwegian University of Science and Technology, Trondheim, Norway.

ISSC. 2003. Report of Specialist Committee V.3: Collision and grounding. Proceedings of International Ship and Offshore Structures Congress, San Diego, USA, 11-15 August.

ISSC. 2012. Report of Specialist Committee V.1: Damage assessment following accidents. Proceedings of International Ship and Offshore Structures Congress, Rostock, Germany, 10-13 September.

Karlsson UB. 2009. Improved collision safety of ships by an intrusion-tolerant inner side shell. *Marine Technology*. 46: 165-173.

Kim YS, Youssef SAM, Ince ST, Kim SJ, Seo JK, Kim BJ, Ha YC, Paik JK. 2015. Environmental consequences associated with collisions involving double hull oil tanker. *Ships and Offshore Structures.* 10(5): 479–487.

Kitamura O. 2000. Buffer bow design for the improved safety of ships. Ship Structure Symposium, Virginia, USA, 13-14 June.

Ko YG, Kim SJ, Sohn JM, Paik JK. 2017. A practical method to determine the dynamic fracture strain in nonlinear finite element method computations of ship-ship collisions. Online published. Available from: https://doi.org/10.1080/17445302.2017.1405584

Kuroiwa T, Kawamoto Y, Kusuba S, Stillman, D. 1995. Numerical Simulation of Collision and Grounding of Ships. Proceedings of the International Conference on Technologies for Marine Environment Preservation (MARIENV'95), Tokyo, Japan, 24-29 September.

Kuroiwa T. 1996. Numerical simulation of actual collision & grounding accidents. Proceedings of International Conference on Design and Methodologies for Collision and Grounding Protection of Ships, San Francisco, USA, 22-23 August.

Le Source H, Couty N, Besnier F, Kammerer C, Legavre H. 2003. LS-DYNA applications in shipbuilding. Proceedings of 4th European LS-DYNA Users Conference, Ulm, Germany, 22-23 May.

Liu B, Villavicenco R, Soares CG. 2013. Experimental and numerical plastic response and failure of laterally impacted rectangular plates. *Journal of Offshore Mechanics and Arctic Engineering*. 135: 1-7.

Montewka J, Goerlandt F, Ehlers S, Kunjala P, Erceg S, Polic D, Klanac A, Hinz T, Tabri K. 2012. A model for consequence evaluation of ship-ship collision based on Bayesian belief network. In: *Sustainable Maritime Transportation and Exploitation of Sea Resources*. Edited by E. Rizzuto and C. Guedes Soares, CRC Press, New York, USA.

Ozguc O, Das PK, Barltrop N. 2005. A comparative study on the structural integrity of single and double side skin bulk carriers under collision damage. *Marine Structures*. 18: 511-547.

Parunov J, Rudan S, Corak M. 2016. Ultimate hull-girder-strength-based reliability of a double-hull oil tanker after collision in the Adriatic Sea. *Ships and Offshore Structures.* 12(S1): S55-S67.

Paik JK, Pedersen PT. 1995. On design of double hull tankers against collisions, Proceedings of 6th International Symposium on Practical Design of Ships and Mobile Units, Seoul, Korea, 17-22 September.

Paik JK. 2007a. Practical techniques for finite element modeling to simulate structural crashworthiness in ship collisions and grounding (Part I: Theory). *Ships and Offshore Structures*. 2(1): 69-80.

Paik JK. 2007b. Practical techniques for finite element modeling to simulate structural crashworthiness in ship collisions and grounding (Part II: Verification). *Ships and Offshore Structures*. 2(1): 81-86.

Paik JK, Thayamballi AK. 2003. Ultimate limit state design of steel plated structures. Wiley, Chichester, UK.

Paik JK, Thayamballi AK. 2007. Ship-shaped offshore installation: design, building and operation. Cambridge University Press, Cambridge, UK.

Paik JK, Park JH, Samuelides E. 2009. Collision accidental limit states performance of double hull oil tanker structures: Pre-CSR versus CSR designs. *Marine Technology*. 46: 183-191.

Pedersen PT. 1993. Ship impacts: Bow collision. *International Journal of Impact Engineering*. 13: 163-187.

Pedersen PT, Zhang S. 1998. On impact mechanics in ship collisions. *Marine Structures*. 11(10): 429-449.

Sajdak J, Brown A. 2004. Modeling longitudinal damage in ship collisions. SSC-437, Ship Structure Committee, Washington DC, USA.

Simonsen BC. 1997. Mechanics of ship grounding [PhD thesis]. Technical University of Denmark, Lyngby, Denmark.

Storheim M, Amdahl J. 2014. Design of offshore structures against accidental ship collisions. *Marine Structures.* 37: 135-172.

Storheim M, Amdahl J. 2015. On the sensitivity to work hardening and strain-rate effects in nonlinear FEM analysis of ship collisions. *Ships and Offshore Structures.* 12(1): 100-115.

Storheim M, Alsos HS, Hopperstad OS, Amdahl J. 2015. A damage-based failure model for coarsely meshed shell structures. *International Journal of Impact Engineering.* 83: 59-75.

Tavakoli MT, Amdahl J, Leira BJ. 2010. Analytical and numerical modelling of oil spill from a side tank with collision damage. *Ships and Offshore Structures.* 7(1): 73-86.

Tornqvist R. 2003. Design of crashworthy ship structures [PhD thesis]. Technical University of Denmark, Lyngby, Denmark.

Urban J. 2003. Crushing and fracture of lightweight structures [PhD thesis]. Technical University of Denmark, Lyngby, Denmark.

Villavicenco R, Kim YH, Cho SR, Guedes Soares C. 2013. Deformation process of web girders in small-scale tanker double hull structures subjected to lateral impact. *Marine structures.* 32: 84-112.

Wierzbicki T, Abramowicz W. 1983. On the crushing mechanics of thin-walled structures. *Journal of Applied Mechanics.* 50: 727-734.

Wisniewski K, Kolakowski P. 2002. The effect of selected parameters on ship collision results by dynamic FE simulations. *Finite Elements in Analysis and Design.* 39: 985-1006.

Yamada Y, Endo H. 2008. Experimental and numerical study on the collapse strength of the bulbous bow structure in oblique collision. *Marine Technology.* 45: 42–53.

Youssef SAM, Faisal M, Seo JK, Kim BJ, Ha YC, Kim DK, Paik JK, Cheng F, Kim MS. 2014. Assessing the risk of ship hull collapse due to collision. *Ships and Offshore Structures.* 11(4): 335-350.

Youssef SAM, Noh SH, Paik JK. 2017. A new method for assessing the safety of ships damaged by collisions. *Ship and Offshore Structures.* (http://dx.doi.org/10.1080/17445302.2017.1285679)

Zhang S. 1999. The mechanics of ship collisions [PhD thesis]. Technical University of Denmark, Lyngby, Denmark.

Zhang S, Villavicencio R, Zhu L, Pedersen PT. 2016. Impact mechanics of ship collisions and validations with experimental results. *Marine structures*. 52: 69-81.

Zheng Y, Aksu D, Vassalos, Tuzcu C. 2007. Study on side structure resistance to ship-ship collision. *Ships and Offshore Structures.* 2(3): 273-293.

Appendix A. Results of Collision Consequence Analysis
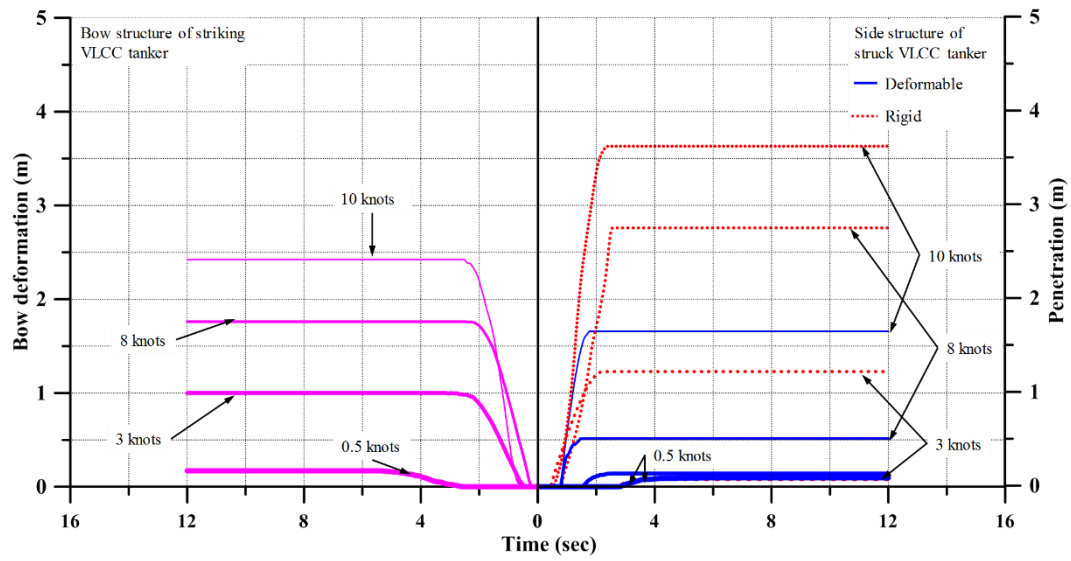
(a) The behavior of penetration with time
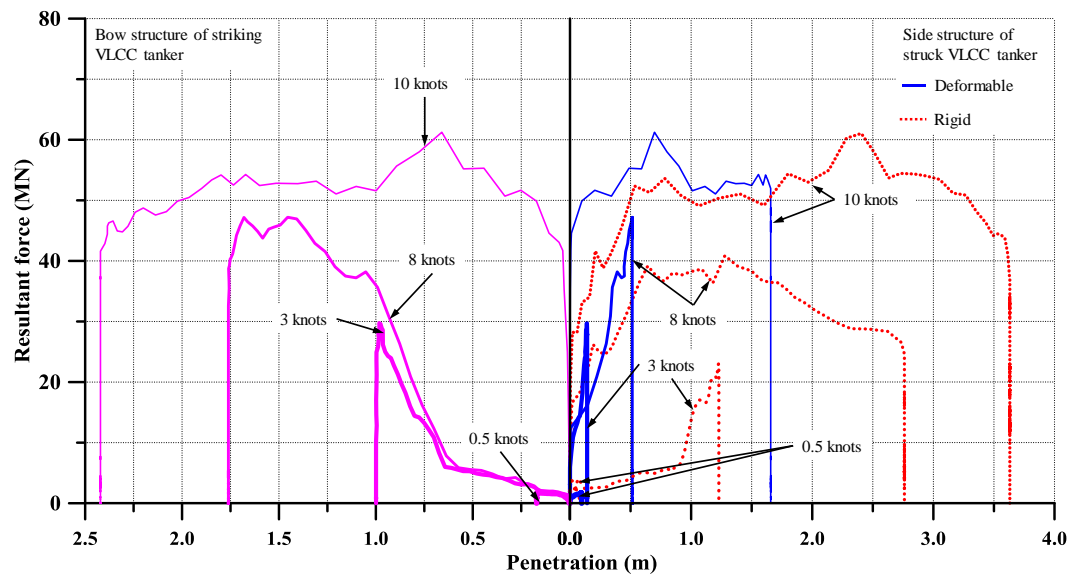
(b) The behavior of resultant forces with time

Figure A (1). The effects of the deformable and rigid striking VLCC tanker at a collision angle of 45 deg.
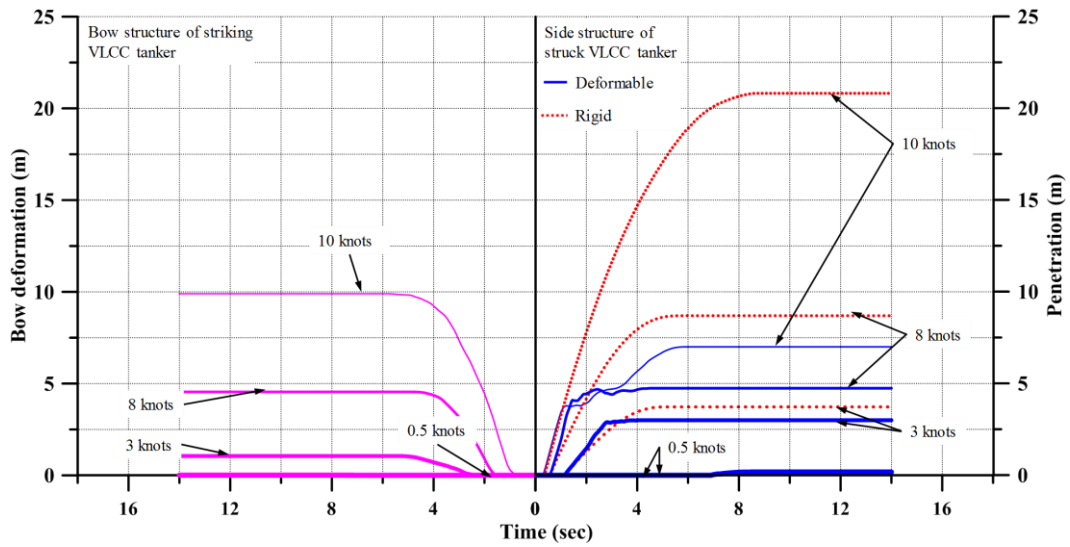
(a) The behavior of penetration with time
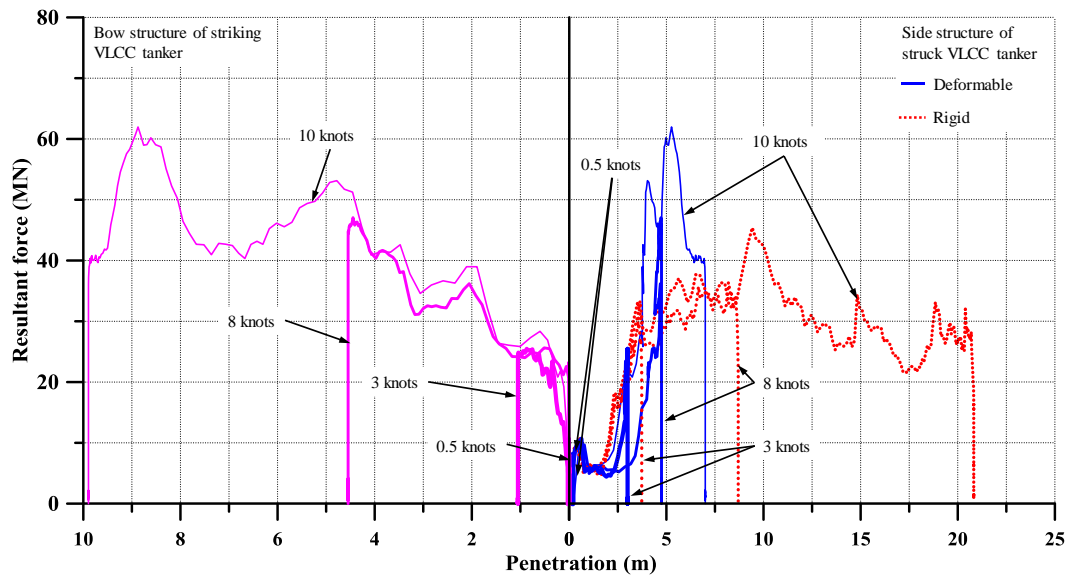
(b) The behavior of resultant forces with time

Figure A (2). The effects of the deformable and rigid striking VLCC tanker at a collision angle of 90 deg.
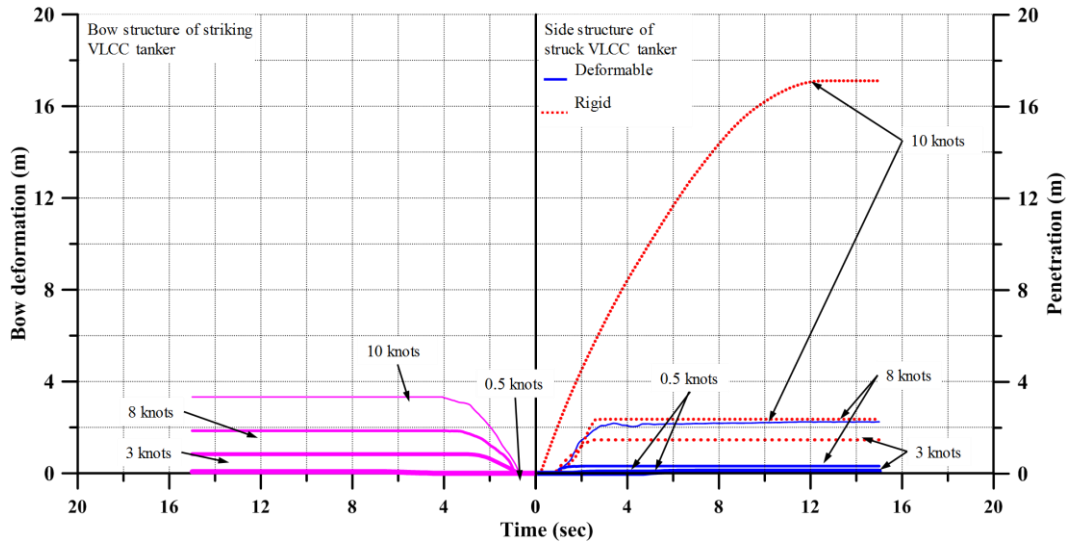
(a)   The behavior of penetration with time
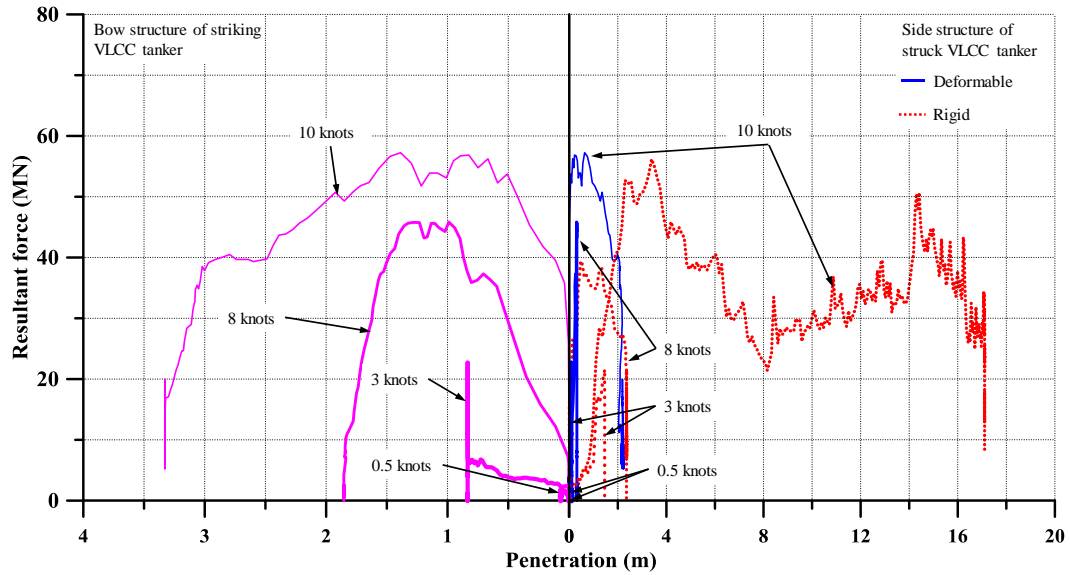
(b)   The behavior of resultant forces with time

Figure A (3). The effects of the deformable and rigid striking VLCC tanker at a collision angle of 135 deg.
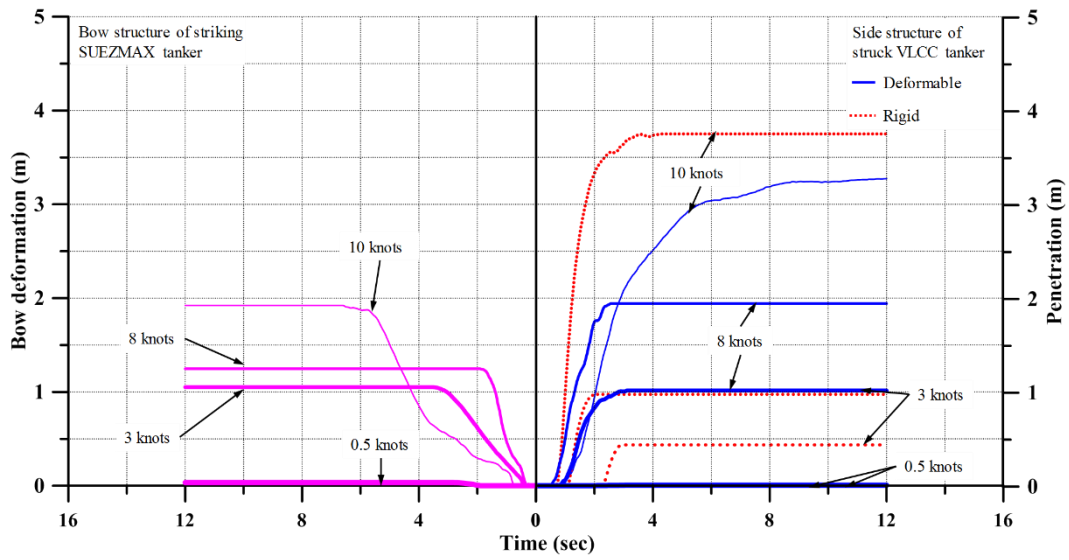
(a)   The behavior of penetration with time
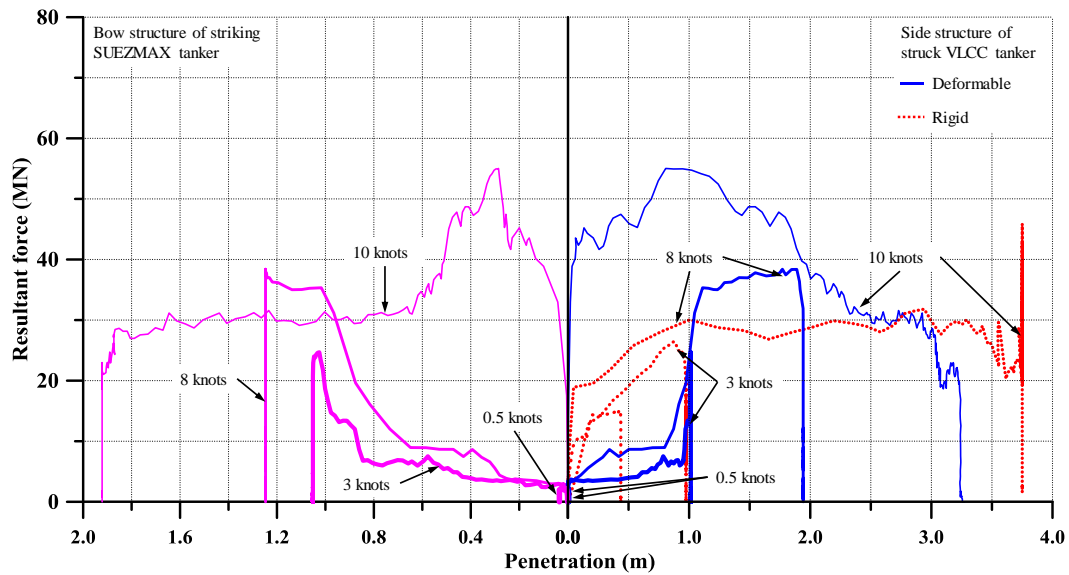
(b)   The behavior of resultant forces with time

Figure A (4). The effects of the deformable and rigid striking SUEZMAX tanker at a collision angle of 45 deg.
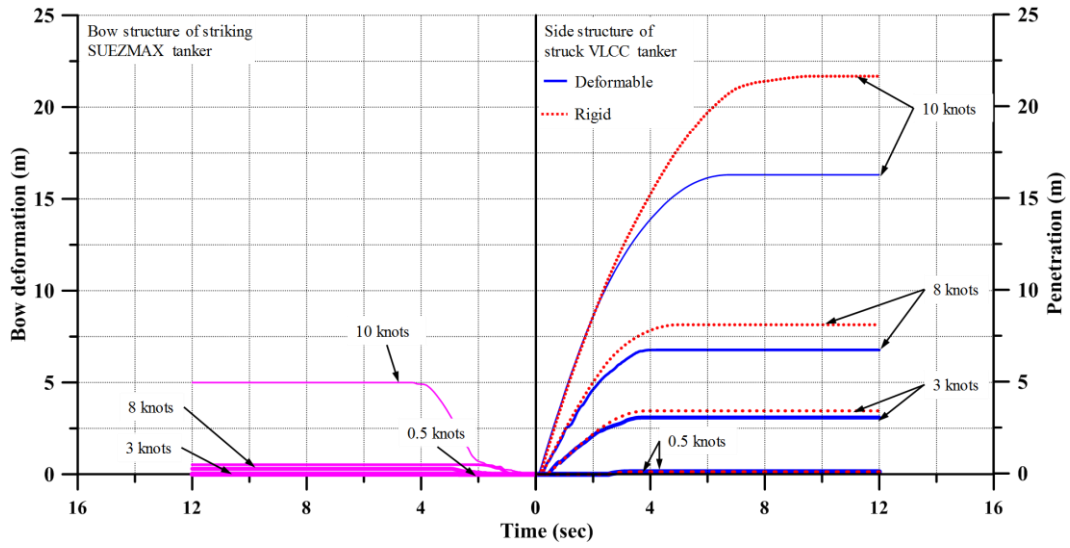
(a) The behavior of penetration with time
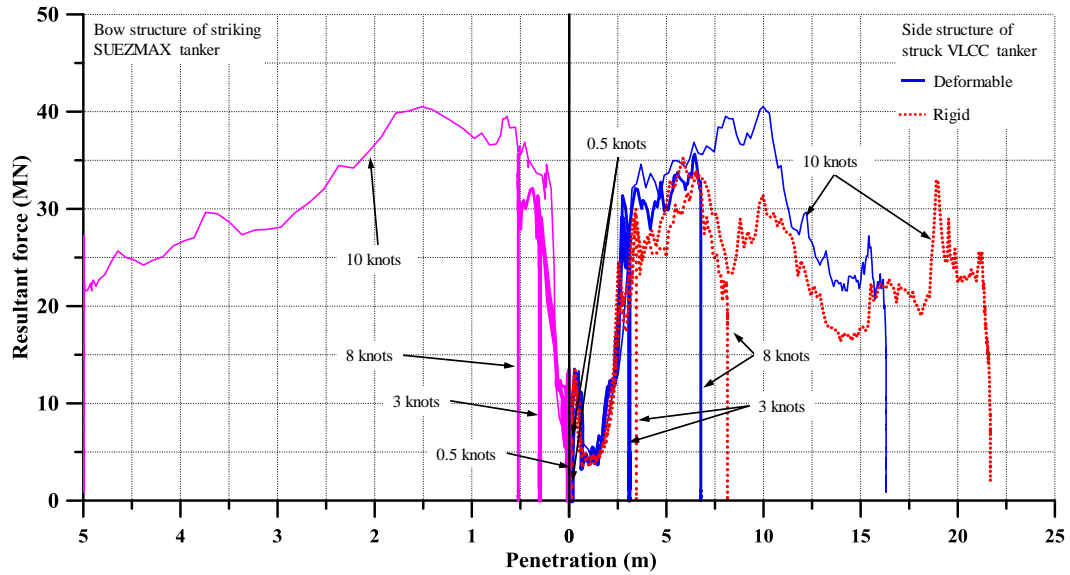
(b) The behavior of resultant forces with time

Figure A (5). The effects of the deformable and rigid striking SUEZMAX tanker at a collision angle of 90 deg.
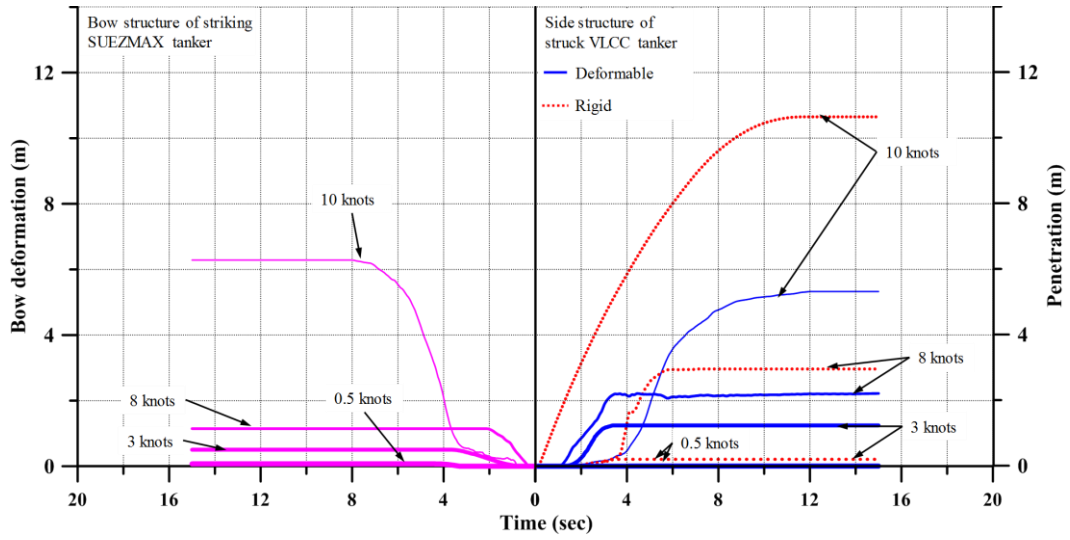
(a) The behavior of penetration with time
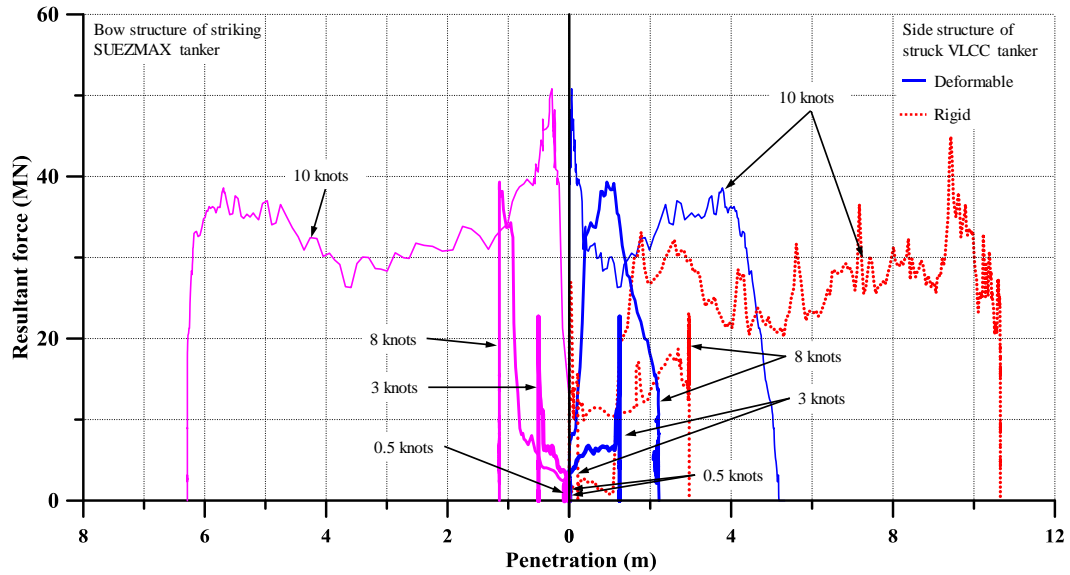
(b) The behavior of resultant forces with time

Figure A (6). The effects of the deformable and rigid striking SUEZMAX tanker at a collision angle of 135 deg.

Appendix B. Maximum Results of Collision Consequence Analysis at Each Collision Angle
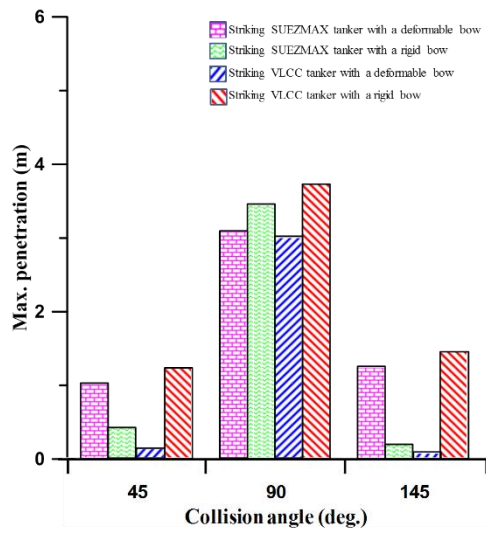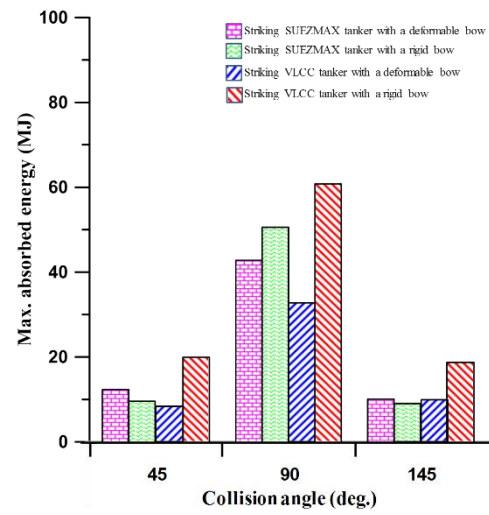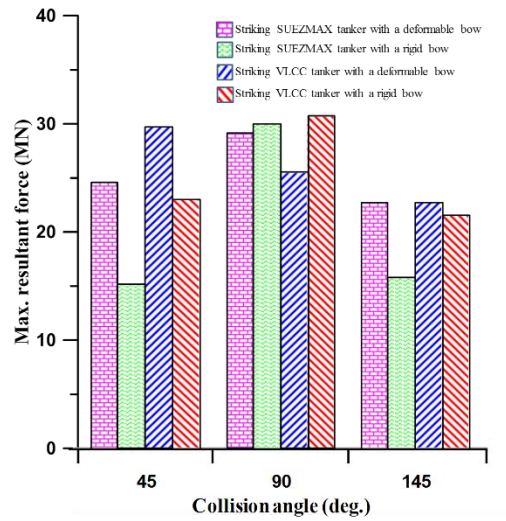

(a)

(b)

(c)
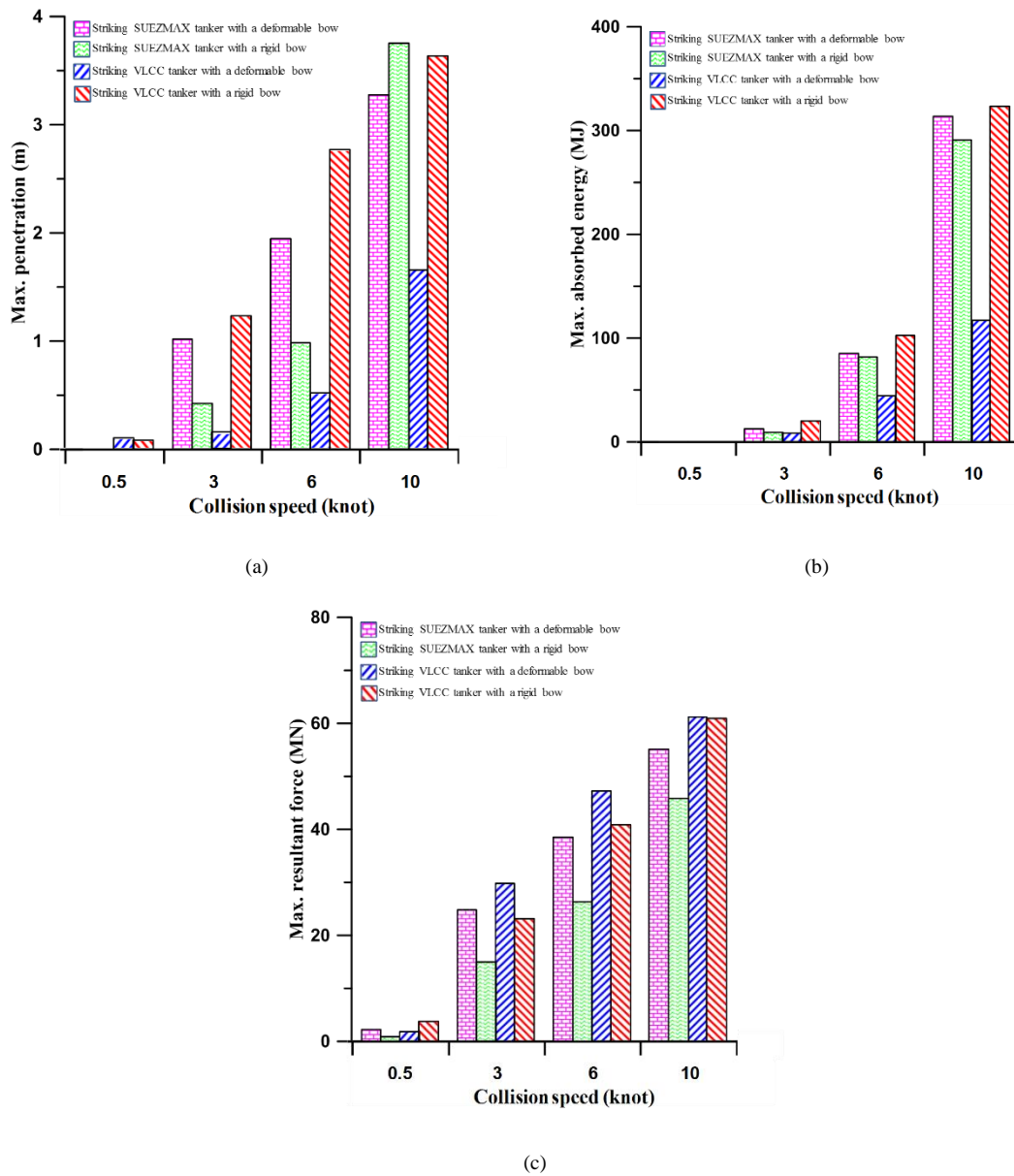
Figure B (1). The behaviors of the deformable and rigid striking ship bow on the maximum penetration, maximum absorbed energy and maximum resultant force at a collision angle of 45 deg.
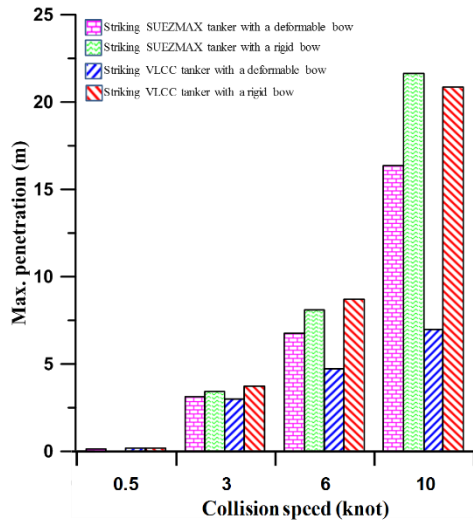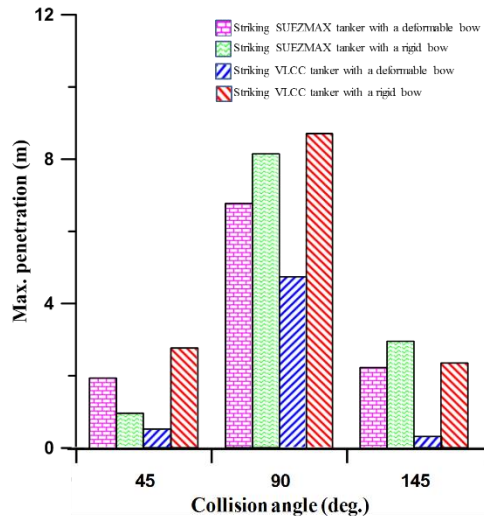
(a)
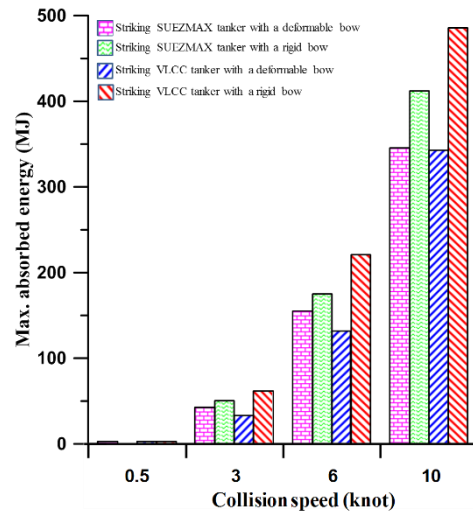
(b)
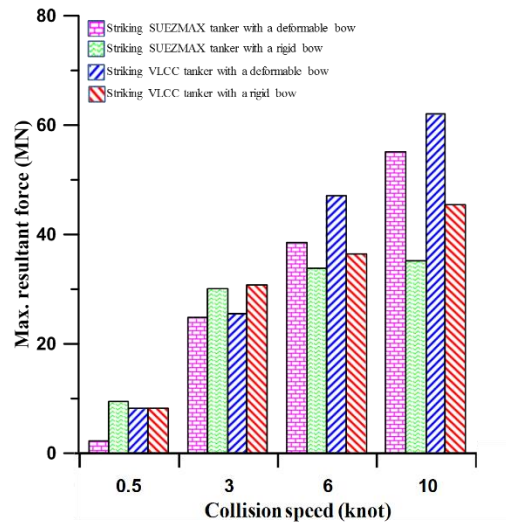
(c)

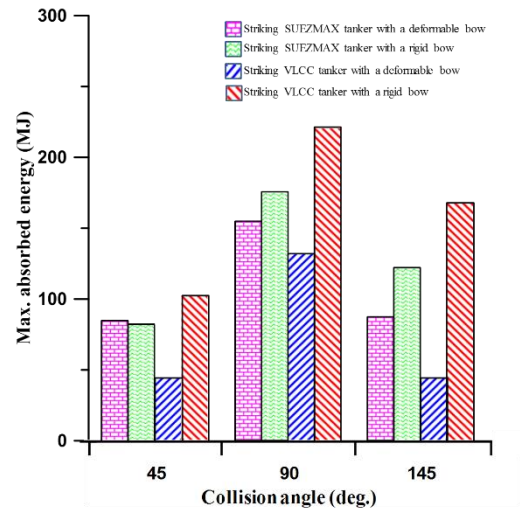**Figure B (2).** The behaviors of the deformable and rigid striking ship bow on the maximum penetration, maximum absorbed energy and maximum resultant force at a collision angle of 90 deg.
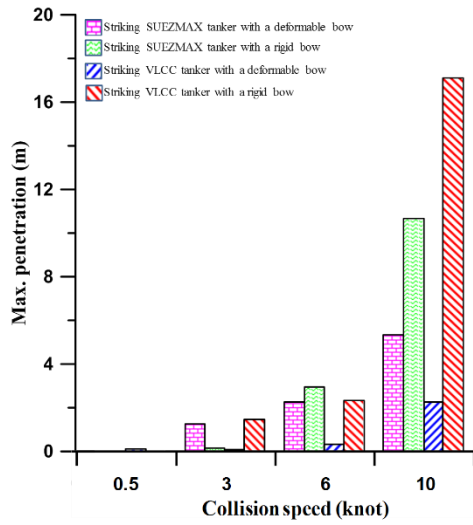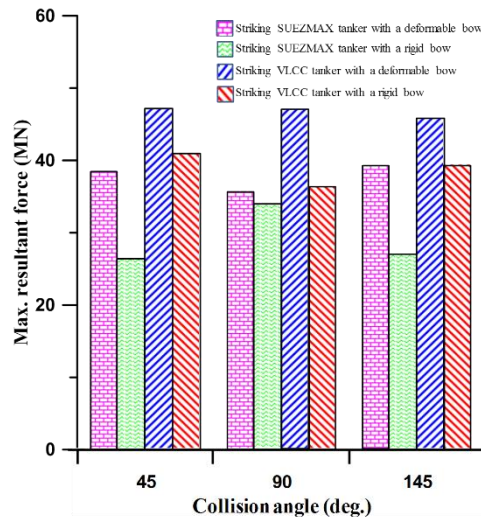
(a)
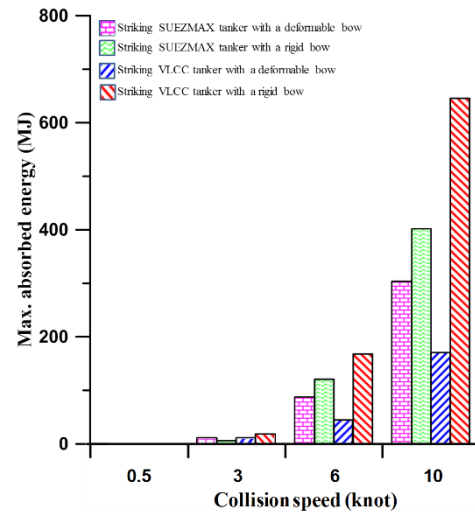
(b)
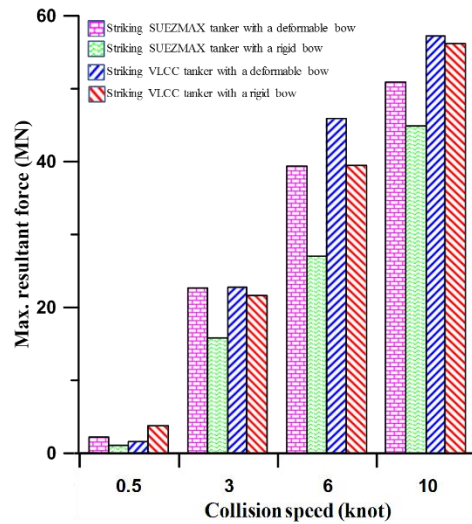
(c)

Figure B (3). The behaviors of the deformable and rigid striking ship bow on the maximum penetration, maximum absorbed energy and maximum resultant force at a collision angle of 135 deg.

Appendix C. Maximum Results of Collision Consequence Analysis at Each Collision Velocity

(a)

(b)

(c)
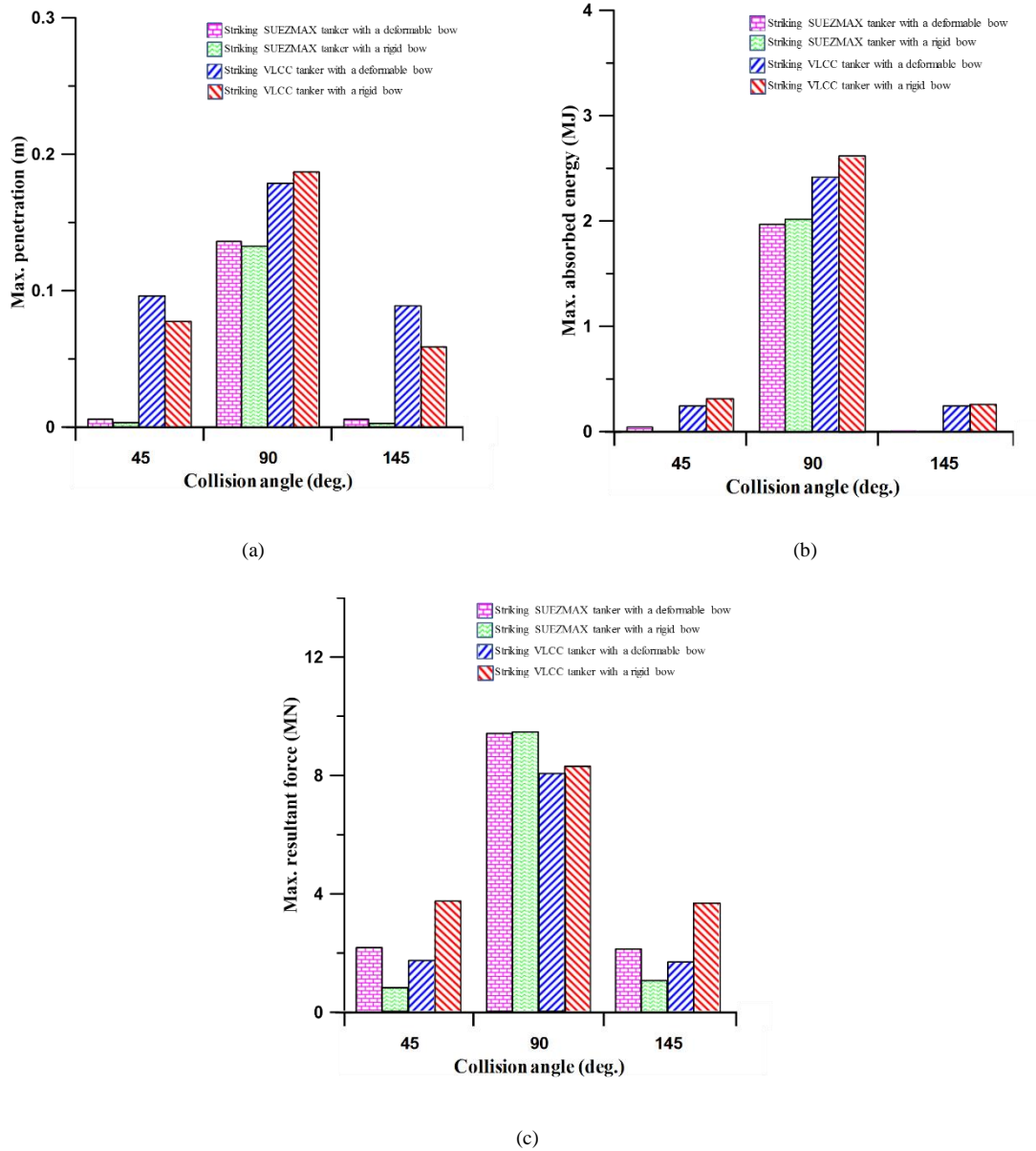
Figure C (1). The behaviors of the deformable and rigid striking ship bow on the maximum penetration, maximum absorbed energy and maximum resultant force at a collision speed of 0.5 knots.

Figure C (2). The behaviors of the deformable and rigid striking ship bow on the maximum penetration, maximum absorbed energy and maximum resultant force at a collision speed of 3 knots.
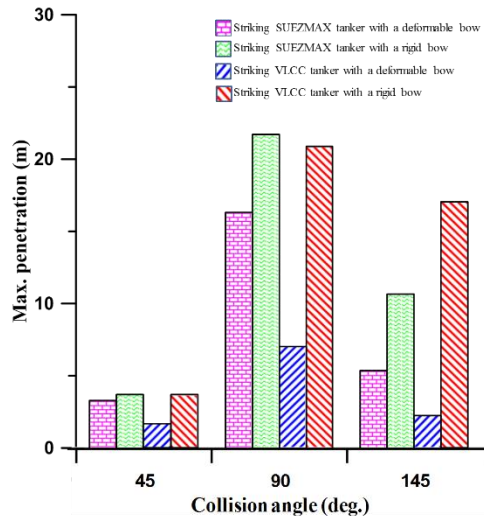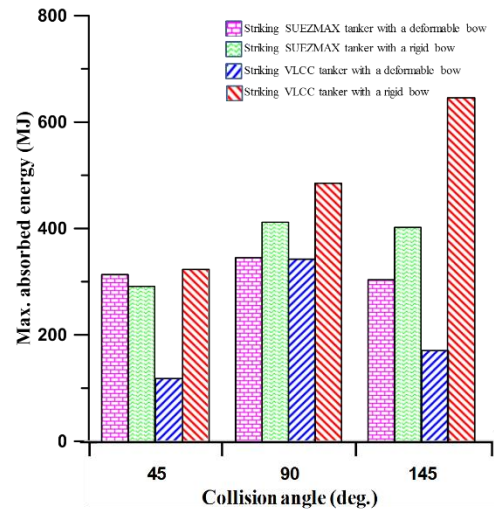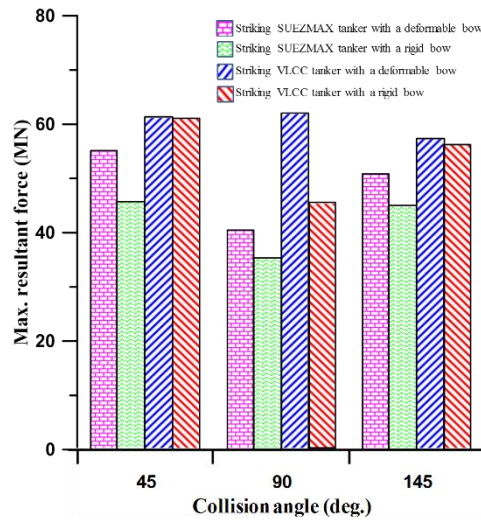
(a)

(b)

(c)

Figure C (3). The behaviors of the deformable and rigid striking ship bow on the maximum penetration, maximum absorbed energy and maximum resultant force at a collision speed of 6 knots.

Figure C (4). The behaviors of the deformable and rigid striking ship bow on the maximum penetration, maximum absorbed energy and maximum resultant force at a collision speed of 10 knots.